

RESEARCH ARTICLE

Lamb1a regulates atrial growth by limiting second heart field addition during zebrafish heart development

Christopher J. Derrick^{1,*}, Eric J. G. Pollitt¹, Ashley Sanchez Sevilla Uruchurtu^{1,‡}, Farah Hussein¹, Andrew J. Grierson² and Emily S. Noël^{1,§}

ABSTRACT

During early vertebrate heart development, the heart transitions from a linear tube to a complex asymmetric structure, a morphogenetic process that occurs simultaneously with growth of the heart. Cardiac growth during early heart morphogenesis is driven by deployment of cells from the second heart field (SHF) into both poles of the heart. Laminin is a core component of the extracellular matrix and, although mutations in laminin subunits are linked with cardiac abnormalities, no role for laminin has been identified in early vertebrate heart morphogenesis. We identified tissue-specific expression of laminin genes in the developing zebrafish heart, supporting a role for laminins in heart morphogenesis. Analysis of heart development in *lamb1a* zebrafish mutant embryos reveals mild morphogenetic defects and progressive cardiomegaly, and that Lamb1a functions to limit heart size during cardiac development by restricting SHF addition. *lamb1a* mutants exhibit hallmarks of altered haemodynamics, and blocking cardiac contractility in *lamb1a* mutants rescues heart size and atrial SHF addition. Together, these results suggest that laminin mediates interactions between SHF deployment and cardiac biomechanics during heart morphogenesis and growth in the developing embryo.

KEY WORDS: Heart development, Laminin, Extracellular matrix, Second heart field, Zebrafish, Contractility

INTRODUCTION

Tissue morphogenesis requires tight coordination of changes in cell shape and organisation, gene expression and tissue patterning, together with the integration of intrinsic and extrinsic signalling cues. Cardiac development represents an excellent example of such complex morphogenesis, in which the linear heart tube undergoes growth, local tissue deformation and functional regionalisation. The importance and complexity of heart morphogenesis are evident in the prevalence of congenital heart defects (CHDs), which occur in at least 1% of live births and are the leading cause of birth defect-related deaths worldwide (Triedman and Newburger, 2016).

Heart looping and chamber ballooning are key stages in cardiac development, during which the heart tube undergoes a complex

morphological rearrangement resulting in a helical looped tube in mouse and a planar looped tube in zebrafish (*Danio rerio*) (Desgrange et al., 2018). This is concomitant with an increase in myocardial cell number, primarily achieved through cell addition to the poles of the developing heart from a progenitor pool in the adjacent mesoderm, termed the ‘second heart field’ (SHF) (Kelly, 2012). During cardiogenesis in mouse and chick, SHF addition generates a significant proportion of cardiac tissue, including the right ventricle, atria and inflow and outflow tracts (OFT) (Kelly et al., 2001; Mjaatvedt et al., 2001; Waldo et al., 2001). In zebrafish, the SHF makes a similar contribution to the inflow tract at the base of the atrium, the single ventricle and the OFT (Hami et al., 2011; Lazic and Scott, 2011; de Pater et al., 2009; Zhou et al., 2011). The signaling pathways required for SHF addition are highly conserved across vertebrates (Knight and Yelon, 2016; Rochais et al., 2009), with *Fgf8* promoting SHF addition and an opposing retinoic acid (RA) gradient limiting SHF addition to the arterial pole (Ryckebusch et al., 2008; Rydeen and Waxman, 2016; Zaffran et al., 2014). SHF addition and cardiac morphogenesis are tightly linked, with defects in SHF addition leading to heart malformations and congenital heart disease (Francou and Kelly, 2016).

Mechanical forces are also linked with SHF addition. Recent studies demonstrated that the SHF epithelium is under tension, which is proposed to regulate cell orientation and cell division, driving extension of the linear heart tube (Francou et al., 2017); it has also been suggested that heart tube contractility could contribute to this tension. Finally, because heart function begins once the heart tube is formed, cardiomyocyte contractility, blood flow, SHF addition and morphogenesis all occur simultaneously (Beis et al., 2005; Dietrich et al., 2014; Heckel et al., 2015; Kalogirou et al., 2014; Samsa et al., 2015; Vermot et al., 2009), resulting in a complex interplay of biochemical and biomechanical cues driving robust heart morphogenesis.

The extracellular matrix (ECM) is an important signalling centre that influences biochemical signalling between cells and provides biomechanical stimuli. Numerous studies have highlighted the importance of the cardiac ECM during heart development (Derrick and Noël, 2021); however, comparatively little is known about the specific roles that individual ECM components play in promoting heart looping, chamber morphogenesis and cardiac growth. Laminins are large heterotrimeric complexes deposited early during ECM construction. Consisting of an alpha, beta and gamma chain, laminin trimers are an essential component of the basement membrane, where they interact with integrin receptors on the cell membrane and facilitate ECM organisation in the interstitial matrix (Domogatskaya et al., 2012; Mouw et al., 2014). Multiple alpha, beta and gamma subunits are encoded in the genome and assemble into a variety of trimer isoforms, which often exhibit tissue-restricted expression and play specific roles in different tissue contexts (Schéele et al., 2007). Previous studies suggest that

¹Department of Biomedical Science, University of Sheffield, Sheffield S10 2TN, UK.

²Sheffield Institute for Translational Neuroscience, University of Sheffield, Sheffield S10 2HQ, UK.

*Present address: Biosciences Institute, Faculty of Biomedical Sciences, Newcastle University, International Centre for Life, Central Parkway, Newcastle upon Tyne NE1 3BZ, UK. †Present address: Division of Biology and Medicine, Brown University, Providence, RI 02912, USA.

[§]Author for correspondence (e.s.noel@sheffield.ac.uk)

ORCID: C.J.D., 0000-0002-5008-3014; E.J.G.P., 0000-0003-2406-2241; A.S., 0000-0002-1979-1805; F.H., 0000-0003-4241-5805; A.J.G., 0000-0001-7039-6731

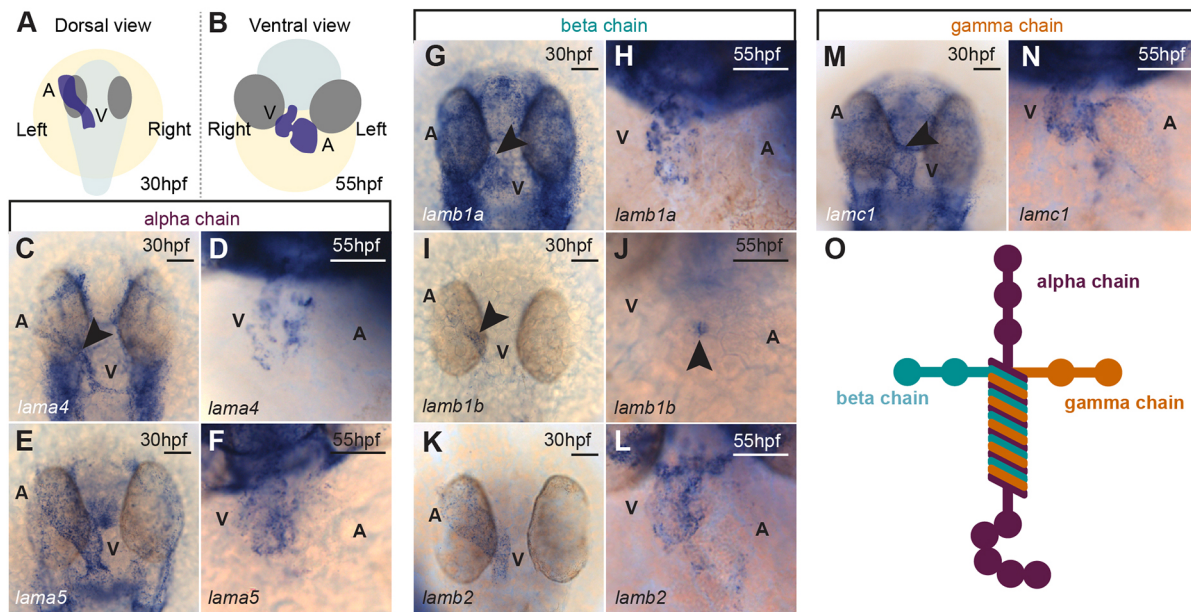


Fig. 1. Dynamic expression of laminin subunit genes during heart morphogenesis. (A,B) Schematic of the position of the heart (blue) in a 30 hpf zebrafish embryo (A; dorsal view) and a 55 hpf zebrafish embryo (B; ventral view). The embryo body is shaded pale grey, eyes are shaded dark grey and the yolk is shaded in yellow. (C-F) mRNA *in situ* hybridisation expression analysis of laminin alpha chain subunits *lama4* (C,D) and *lama5* (E,F) in the heart. (G-L) mRNA *in situ* hybridisation expression analysis of laminin beta subunit chains *lamb1a* (G,H), *lamb1b* (I,J) and *lamb2* (K,L) in the heart. (M,N) mRNA *in situ* hybridisation expression analysis of gamma subunit *lamc1* in the heart. Arrowheads indicate the position of the heart and the anterior is to the top in all images. (O) Schematic of the heterotrimeric structure of laminin. Scale bars: 50 μ m. A, atrium; V, ventricle.

laminins have important roles in human heart development and function. Deleterious mutations in *LAMA4* have been identified in patients with dilated cardiomyopathy (Knöll et al., 2007), a mutation in *LAMA5* has been associated with a multi-systemic disorder that includes cardiac abnormalities (Sampaolo et al., 2017), and ~30% of patients with Dandy–Walker Syndrome (DWS), a rare brain malformation linked to mutations in *LAMC1*, also present with CHDs (Darbro et al., 2013). Although these studies suggest requirements for laminins in cardiac form and function, mechanistically little is known about the roles that they play during cardiac morphogenesis. Direct evidence supporting a role for laminins in heart development comes from *Drosophila*, in which laminins promote the formation and integrity of the dorsal vessel (Haag et al., 1999; Yarnitzky and Volk, 1995). Current vertebrate models have provided limited insights into the role of laminins in cardiac development. *Lama4* mutant mice survive postpartum without overt cardiac defects, although, over time, pups develop enlarged hearts with larger cardiomyocytes (Thyboll et al., 2002; Wang et al., 2006). However, interrogating the role of laminins more broadly in heart development is challenging because of the early lethality in both *Lamc1* and *Lamb1* mutant mice (Miner et al., 2004; Smyth et al., 1999).

In this study, we identify two novel functions for laminins during heart development in zebrafish, promoting heart looping morphogenesis and restricting cardiac size. We show that *Lamb1a* controls cardiac growth by limiting SHF addition and demonstrate that excessive atrial SHF addition to the venous pole in *lamb1a* mutants is rescued by blocking heart contractility. Finally, we demonstrate that loss of *lamb1a* disrupts expression of RA-responsive genes in the heart in a contractility-dependent manner, supporting a role for laminins in coupling mechanical force, intercellular signalling and cardiac growth. Thus, this study presents the first reported role for laminins in early vertebrate heart development.

RESULTS

Laminins display dynamic, tissue-specific expression during early zebrafish heart morphogenesis

To investigate the role of laminin complexes in early vertebrate heart morphogenesis, we probed a previously published transcriptomic analysis of cardiac gene expression to identify laminin subunit genes expressed in the heart tube (Derrick et al., 2021) and, in combination with an *in situ* hybridisation screen, identified a subset of laminin subunits with cardiac expression during early stages of heart looping (Fig. 1; Fig. S1).

At 30 hours post fertilisation (hpf) (Fig. 1A), during early heart tube morphogenesis, six laminin subunits are expressed in the zebrafish heart: two alpha chains (*lama4* and *lama5*; Fig. 1C,E); three beta chains (*lamb1a*, *lamb1b* and *lamb2*; Fig. 1G,I,K) and a single gamma chain (*lamc1*; Fig. 1M). Given that specific laminin isoforms can exhibit tissue-specific deposition, we carried out two-colour fluorescent *in situ* hybridisation at 30 hpf to identify whether the myocardium and endocardium have a specific laminin expression profile (Fig. S1). This identified two laminin genes expressed in the endocardium *lama4* and *lamb1b* (Fig. S1A,B); two laminin genes expressed in the myocardium: *lama5* and *lamb2* (Fig. S1C,D); and two laminin subunits expressed in both myocardium and endocardium: *lamb1a* and *lamc1* (Fig. S1E,F).

Whereas at 30 hpf the majority of laminin genes were expressed along the length of the heart tube, following initial heart looping morphogenesis at 55 hpf (Fig. 1B), the expression of most laminin subunits became restricted to the ventricle and atrioventricular canal (Fig. 1D,F,H,L,N), with the exception of *lamb1b*, which was expressed only in the atrioventricular canal (Fig. 1J). This dynamic, spatiotemporal control of specific laminin subunit expression during early heart development suggests that individual endocardial- or myocardial-derived laminin complexes may play a role in early heart morphogenesis.

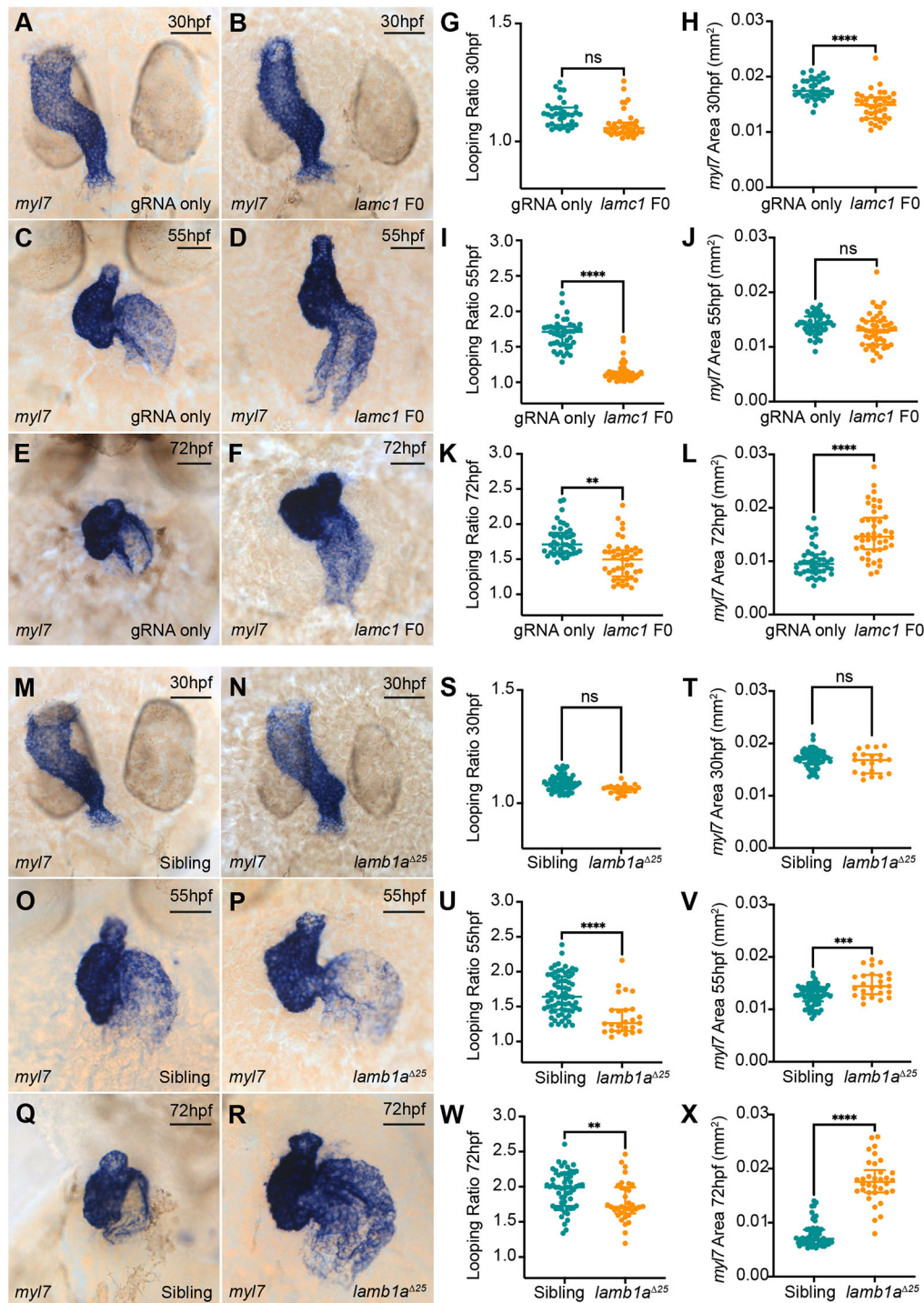


Fig. 2. Laminins perform multiple roles during zebrafish heart morphogenesis. (A-F) mRNA *in situ* hybridisation analysis of *myl7* expression in control embryos injected with *lamc1*-targeting gRNAs only (A,C,E) or with *lamc1*-targeting gRNAs together with Cas9 protein (*lamc1* F0; B,D,F) at 30 hpf (A,B), 55 hpf (C,D) and 72 hpf (E,F).

(G-L) Quantitative analysis of looping ratio (G,I,K) and *myl7* area (H,J,L) in gRNA-injected controls (30 hpf: $n=34$; 55 hpf: $n=44$; 72 hpf: $n=44$) and *lamc1* F0 crispants (30 hpf: $n=38$; 55 hpf: $n=47$; 72 hpf: $n=44$). *lamc1* crispants exhibit reduced heart looping at 55 hpf and 72 hpf, a reduced area of *myl7* expression at 30 hpf and an increased area of *myl7* expression at 72 hpf. Data are median \pm interquartile range, analysed with the Kruskal-Wallis test. (M-R) mRNA *in situ* hybridisation analysis of *myl7* expression in siblings (M,O,Q) and *lamc1a* ^{Δ 25} mutants (N,P,R) at 30 hpf, 55 hpf and 72 hpf. (S-X) Quantitative analysis of looping ratio (S,U,W) and *myl7* area (T,V,X) in siblings (30 hpf: $n=65$; 55 hpf: $n=70$; 72 hpf: $n=56$) and *lamc1a* ^{Δ 25} mutants (30 hpf: $n=20$; 55 hpf: $n=25$; 72 hpf: $n=34$). *lamc1a* ^{Δ 25} mutants exhibit a mild reduction in heart looping from 55 hpf, and an increased area of *myl7* expression at 55 hpf and 72 hpf. Data are median \pm interquartile range, S-W were analysed with the Mann-Whitney U test, X was analysed with the Kruskal-Wallis test. **** $P<0.0001$, *** $P<0.001$, ** $P<0.01$, ns=not significant in all graphs. Scale bars: 50 μ m.

lamc1 and *lamc1a* regulate heart morphology and size during development

Having identified potential laminin complexes expressed in the heart during early morphogenesis, we examined the role of laminins during heart development. Laminins are heterotrimeric complexes comprising single alpha, beta and gamma chains (Fig. 1O), which are assembled intracellularly prior to deposition into the ECM; thus, the removal of a single subunit is sufficient to prevent extracellular secretion of the complex (Yurchenco et al., 1997). Therefore, to investigate the requirement for laminins during heart looping morphogenesis, we targeted the single gamma subunit *lamc1*,

expressed in both the myocardium and endocardium (Fig. 1M,N; Fig. S1F). Using CRISPR-Cas9 mutagenesis, we generated transient F0 *lamc1* mutants (F0/crispant) (Burger et al., 2016). *lamc1* crispants recapitulated the morphological phenotype of stable *lamc1* mutants with high efficacy, whereas uninjected embryos or injection controls [guide RNA (gRNA) only or Cas9 only] were morphologically normal (Fig. S2A-D) (Odenthal et al., 1996; Parsons et al., 2002). *lamc1* crispants formed a beating heart tube by 26 hpf and, at 2 days post fertilisation (dpf), exhibited mild pericardial oedema, suggesting defects in heart looping morphogenesis (Fig. S2D). We assessed the impact of loss of Lamc1 on heart morphology by *myl7* expression

analysis (Fig. 2A-F), quantifying looping ratio and heart size at 30 hpf, 55 hpf and 72 hpf (Fig. 2G-L; Fig. S2E-F). *lamc1* crispant heart tubes were smaller than control hearts at 30 hpf (Fig. 2A,B,H) and, at 55 hpf, *lamc1* crispants had failed to undergo correct heart looping morphogenesis (Fig. 2C,D), displaying a significant reduction in heart looping ratio compared with controls (Fig. 2I). Interestingly, *lamc1* crispant hearts were of comparable size to those of their control siblings at 55 hpf (Fig. 2J) whereas, by 72 hpf, in addition to abnormal cardiac morphology (Fig. 2F,K; Fig. S2E), *lamc1* crispant hearts appeared significantly larger than those in controls (Fig. 2E,L; Fig. S2F). These results reveal that laminins promote initial heart looping and might regulate cardiac size throughout morphogenesis.

Distinct laminin complexes play varied yet specific roles in different developmental contexts (Schéele et al., 2007). Given that *lambla* exhibited similar expression dynamics and tissue specificity as *lamc1* (Fig. 1; Fig. S1), this suggested that *Lambla* and *Lamc1* may form part of the laminin complexes required for heart development. To investigate this, we generated two stable mutant alleles, *lambla*^{Δ19} and *lambla*^{Δ25}, using CRISPR-Cas9-mediated genome editing (Fig. S2G-M). In contrast to *lamc1* crispants, at 30 hpf, *lambla*^{Δ25} mutant hearts were comparable in size to their sibling controls (Fig. 2M,N,T). However, at 55 hpf, *lambla* mutants also displayed a mild yet significant reduction in heart looping compared with siblings (Fig. 2O,P,U), although this defect was less severe than that observed in *lamc1* crispants (compare Fig. 2D with Fig. 2P; unpaired *t*-test of looping ratio between mutants: *P*<0.0001). *lambla* mutants also exhibited a mild increase in heart size at 55 hpf (Fig. 2V; Fig. S2N,O,R), a progressive defect resulting in significantly cardiomegaly at 72 hpf (Fig. 2Q,R,X; Fig. S2P,Q,S). Although mutant alleles for both *lamc1* and *lambla* have been previously described (Hochgreb-Hägele et al., 2013; Odenthal et al., 1996; Parsons et al., 2002), defects in heart development have not been reported. Analysis of heart morphology in *grumpy*^{ij299a} (*gup*, *lambla*) and *sleepy*^{sa379} (*sly*, *lamc1*) mutants revealed similar phenotypes to our loss-of-function models (Fig. S3), although *lambla*^{Δ25} mutants presented with slightly more severe defects in looping morphology at 55 hpf compared with *grumpy*^{ij299a} mutants. Together, these data demonstrate two previously uncharacterised requirements for laminins in vertebrate heart morphogenesis: promoting heart looping and restricting cardiac size.

The difference in phenotypes between *lambla* and *lamc1* mutants suggested that other laminin beta subunits may either act during early heart morphogenesis or functionally compensate for loss of *lambla*. We examined the impact of loss of *lambla* on the expression of the other laminin beta 1 paralog (*lamblb*) in the heart at 30 hpf and 55 hpf, revealing a striking upregulation and expansion of *lamblb* expression in *lambla*^{Δ25} mutants (Fig. S4A-D). This suggested that upregulation of *lamblb* could compensate for loss of *lambla* (El-Brolosy et al., 2019), resulting in the weaker looping morphogenesis phenotype in *lambla* mutants compared with loss of *lamc1* models. To investigate this, we generated two *lamblb* promoter deletion alleles: *lamblb*^{Δ183} and *lamblb*^{Δ428} (Fig. S4E,F). We increased *lamblb*;*lambla*^{Δ25} double-heterozygous adult fish to obtain *lamblb*;*lambla*^{Δ25} double-mutant embryos and confirmed the absence of *lamblb* transcript at 30 hpf (Fig. S4G-J). Analysis of heart size and morphology in *lamblb*;*lambla*^{Δ25} double mutants at 55 hpf revealed that loss of *lamblb* did not modify the *lambla* mutant phenotype in particular with respect to looping ratio, demonstrating that, despite its upregulation in *lambla*^{Δ25} mutants, *lamblb* does not compensate for the loss of *lambla* (Fig. S4K-N). We next investigated the expression of another laminin beta subunit, *lambl2*, in *lambla*^{Δ25} mutants. At

both 30 hpf and 55 hpf, *lambl2* expression levels in the hearts of *lambla*^{Δ25} mutants were comparable with those in their siblings (Fig. S5A-D). To rule out the possibility that endogenous *lambl2* compensates for loss of *lambla*, we generated *lambl2* F0 crispants (Fig. S5E), either in a sibling or *lambla*^{Δ25} mutant background. *lambl2* crispants did not exhibit gross morphological defects, in line with previously published *lambl2* mutants (Jacoby et al., 2009), and we used PCR analysis to confirm the successful mutagenesis of the multiple *lambl2* target sites. Similar to our functional analysis of *lamblb*, analysis of heart size and morphology in *lambl2* crispants at 55 hpf revealed that loss of *lambl2* alone did not impact cardiac morphology or size, did not modify the *lambla* cardiac phenotype, and did not recapitulate the *lamc1* crispant looping defect (Fig. S5F-O). Together, these results suggest that *lamc1* and *lambla* may play functionally or temporally different roles in cardiac development, or may represent different dynamics of maternal deposition of *lamc1* and *lambla*.

The progression from reduced heart size at 30 hpf to increased heart size at 72 hpf in *lamc1* crispants (Fig. 2) suggests that laminins may regulate heart size differently at early and late stages of cardiac development, and that the early *lamc1*-dependent requirement for laminin in cardiac size is closely linked to looping morphogenesis. Conversely, *lambla* mutants exhibited relatively mild defects in initial heart looping morphogenesis, but developed pronounced cardiomegaly. This represents an interesting model because defects in heart size are often coupled with a severe impact on looping morphology, such as the loss of cerebral cavernous malformation (CCM) pathway components, in which cardiac chambers are larger, but morphology is also severely disrupted (Mably et al., 2006). Therefore, to understand how laminin regulates the growth of the heart specifically subsequent to tube formation, we focused our analysis on the *lambla* mutant.

***lambla* limits SHF addition**

To determine whether the growth of a specific chamber was impacted by the loss of *lambla*, we examined chamber size at 55 hpf and 72 hpf by analysis of *myh7l* and *myh6* expression in the ventricle and atrium, respectively. *lambla* mutants displayed a significant increase in the size of both chambers (Fig. 3A-F), with progressive enlargement between 55 hpf and 72 hpf, suggesting that laminin limits the growth of both chambers. Two mechanisms could account for increased cardiac size: cardiomyocyte hypertrophy or increased cell number. Given that loss of *lama4* and *integrin-linked kinase* (the intracellular effector of laminin-integrin signalling) in zebrafish has previously been associated with dilated cardiomyopathy (Knöll et al., 2007), this suggested that cardiomegaly in *lambla* mutants may result from enlarged cardiomyocytes. We quantified the internuclear distance in both chambers in wild-type (WT) and *lambla*^{Δ25} mutant *Tg(-5.1myl7:DsRed2-NLS)* embryos [henceforth *Tg(my17:DsRed)*], in which myocardial nuclei express DsRed2, at 55 hpf and 72 hpf (Fig. 3G-I). In contrast to our expectation that loss of *lambla* would result in enlarged cardiomyocytes, *lambla*^{Δ25} mutant embryos did not exhibit increased internuclear distance compared with siblings, demonstrating that *Lambla* is not restricting cardiomyocyte size (Fig. 3J,K). Therefore, we hypothesised that cardiomegaly in *lambla* mutants results from increased cell number; quantification of DsRed-positive cardiomyocytes in sibling and *lambla*^{Δ25} mutant embryos at 55 hpf and 72 hpf revealed a significant increase in atrial cell number in *lambla*^{Δ25} mutant embryos at both stages compared with sibling embryos (Fig. 3L,M). Together, these results suggest that *Lambla* controls atrial size by regulating cell number. Analysis

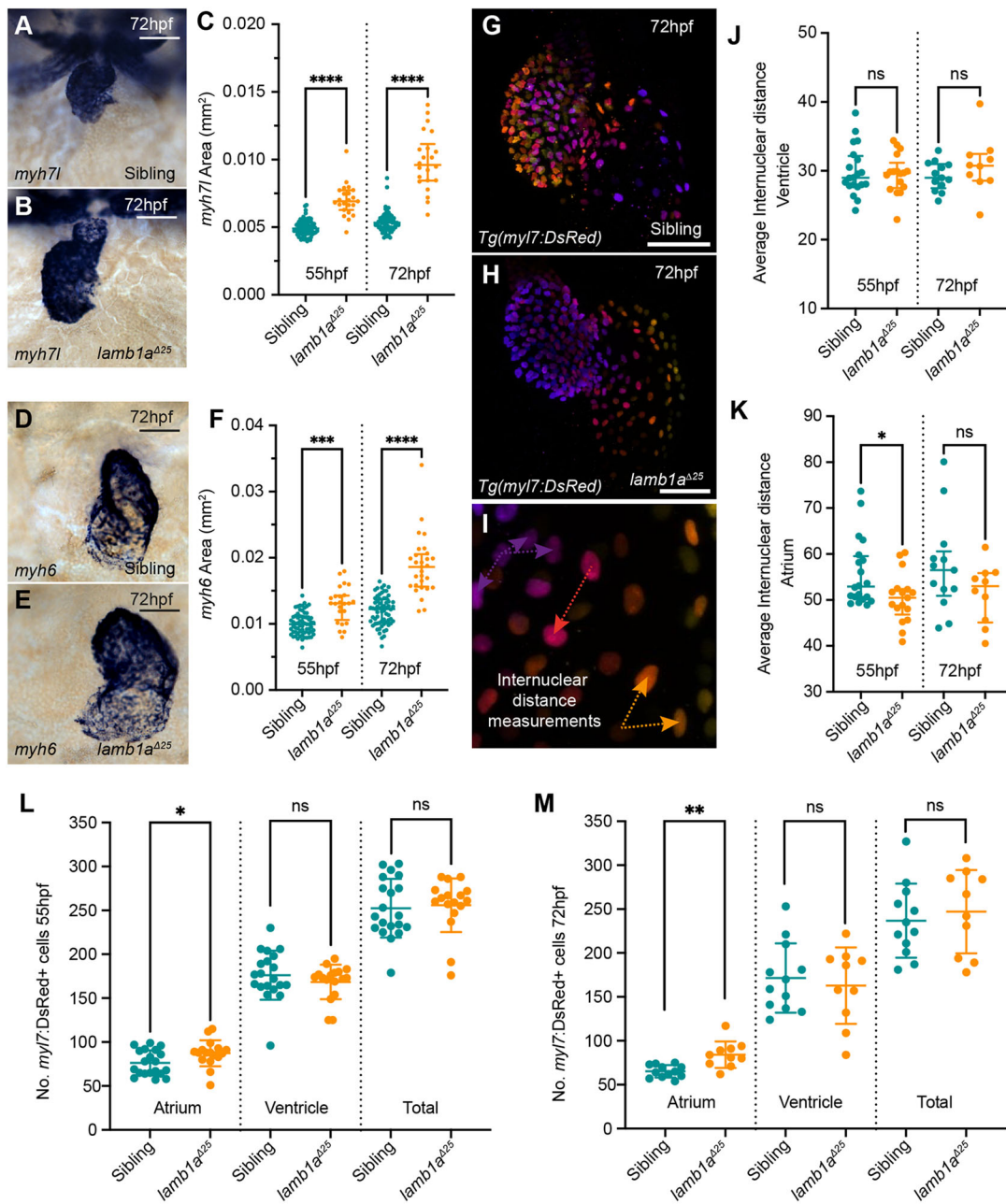


Fig. 3. *lamb1a* mutants have increased atrial cells. (A,B) mRNA *in situ* hybridisation analysis of *myh7l* expression in the ventricle of sibling (A) and *lamb1a*^{A25} mutant embryos (B) at 72 hpf. (C) Quantification of *myh7l* expression area in sibling (55 hpf: $n=72$; 72 hpf: $n=67$) and *lamb1a*^{A25} mutants (55 hpf: $n=23$; 72 hpf: $n=22$). Data are median \pm interquartile range, analysed with the Kruskal–Wallis test. (D,E) mRNA *in situ* hybridisation analysis of *myh6* expression in the atrium of siblings (D) and *lamb1a*^{A25} mutants (E) at 72 hpf. (F) Quantification of *myh6* expression area in siblings (55 hpf: $n=65$; 72 hpf: $n=64$) and *lamb1a*^{A25} mutants (55 hpf: $n=24$; 72 hpf: $n=29$). Data are median \pm interquartile range, analysed with the Kruskal–Wallis test. (G–I) Depth-coded maximum intensity projections of confocal image z-stacks in *Tg(myh7:DsRed)* transgenic sibling (G) and *lamb1a*^{A25} mutants (H) at 72 hpf. Internuclear distance is quantified between nuclei on the same face of the heart that occupy similar z-positions (arrows in I). (J,K) Quantification of average internuclear distance at 55 hpf and 72 hpf in the ventricle (J) and atrium (K) of siblings (55 hpf: $n=20$; 72 hpf: $n=17$) and *lamb1a*^{A25} mutants (55 hpf: $n=13$; 72 hpf: $n=10$), demonstrating a mild decrease in the internuclear distance of *lamb1a*^{A25} mutant atrial cells at 55 hpf (K). Data are median \pm interquartile range, analysed with Brown–Forsythe and Welch ANOVAs with multiple comparisons. (L,M) Quantification of DsRed+ cells in the myocardium of *Tg(myh7:DsRed)* transgenic siblings (55 hpf: $n=20$; 72 hpf: $n=17$) and *lamb1a*^{A25} mutants (55 hpf: $n=13$; 72 hpf: $n=10$) at 55 hpf (L) and 72 hpf (M). *lamb1a*^{A25} mutants have a significant increase in atrial cell number at both stages. Data are mean \pm s.d. Chamber-specific analyses performed with the unpaired *t*-test with Welch’s correction. **** $P<0.0001$, *** $P<0.001$, ** $P<0.01$, * $P<0.05$, ns=not significant in all graphs. Scale bars: 50 μ m.

of DsRed-positive cell number at 30 hpf revealed comparable numbers of cardiomyocytes in *lamb1a*^{A25} mutants and siblings (Fig. S6A–C), suggesting that initial cell number in the heart tube is not affected and that increased cardiomyocyte number in *lamb1a*^{A25} mutants is a progressive defect.

During morphogenesis, the heart grows primarily through addition of cells to the poles of the heart from the SHF. Although previous studies demonstrated that SHF addition to the arterial pole of the heart is sensitive to perturbations in ECM composition (Derrick and Noël, 2021), comparatively less is known about SHF addition to the venous

pole and how the ECM may regulate this process. Given that *lamb1a*^{Δ25} mutants exhibited increased atrial cell number in the heart during the window of SHF addition, we hypothesised that loss of Lamb1a-containing laminin trimers would lead to increased cardiac size through elevated SHF addition. We visualised SHF addition in *Tg(myI7:eGFP);Tg(myI7:DsRed)* double-transgenic sibling and *lamb1a*^{Δ25} mutant embryos, in which cardiomyocytes derived from the linear heart tube/first heart field were marked by both GFP and DsRed expression, whereas cells recently added from the SHF were GFP positive only (de Pater et al., 2009) (Fig. 4C,C'). At 55 hpf, *lamb1a*^{Δ25} mutants appeared to have a larger GFP+;DsRed- area at the poles of the heart, suggesting an increased number of SHF cells (Fig. 4A-B''). Quantification of GFP+;DsRed- cell number in the atrium at 55 hpf revealed a significant increase in SHF cells at the venous pole of *lamb1a*^{Δ25} mutant embryos compared with siblings (Fig. 4D,E), demonstrating that Lamb1a limits atrial size by restricting SHF addition to the venous pole. Analysis of SHF addition to the venous pole of *lamb1a*^{Δ25} mutant hearts at 30 hpf revealed no significant differences compared with siblings (Fig. S6D), suggesting the excess atrial SHF cells in *lamb1a* mutants are added throughout looping morphogenesis. Comparable analysis of cardiomyocyte number in *lamc1* crispants revealed no obvious defects in DsRed+ cell number in the atrium at 55 hpf (Fig. S6E-I) but did suggest an increase in SHF addition to the venous pole (Fig. S6J).

This further supports a role for laminins once the heart tube has formed in regulating SHF addition to the venous pole during looping morphogenesis.

Given that *lamb1a*^{Δ25} mutants also exhibit an increase in ventricular size at 55 hpf (Fig. 3F), we examined SHF addition to the arterial pole of the heart. Cardiomyocytes were more densely packed in the arterial pole than in the venous pole (Fig. 3J,K); therefore, instead of cell number, we quantified the amount of GFP+;DsRed- tissue distal to the first DsRed+ cell in the arterial pole. *lamb1a*^{Δ25} mutants exhibited a significant increase in the amount of GFP+ SHF tissue at the arterial pole (Fig. 4F), suggesting that, similar to the venous pole, laminin limits SHF addition to the ventricle during heart looping morphogenesis.

Increased SHF addition to the atrium of *lamb1a*^{Δ25} mutants could result from a larger SHF progenitor pool at the venous pole. Thus, we examined expression of the transcription factor *islla*, which is expressed in SHF cells and required for SHF addition to the venous pole (de Pater et al., 2009). At both 24 hpf and 55 hpf, the expression domain and levels of *islla* were comparable between *lamb1a*^{Δ25} mutant and sibling embryos (Fig. S7A-D'), demonstrating that increased SHF addition in *lamb1a*^{Δ25} mutants was not the result of enlargement of the SHF domain. Conversely, we observed a mild increase in the ventricular expression of *spry4*, an FGF signalling response gene (Fig. S7E,F), in line with previous

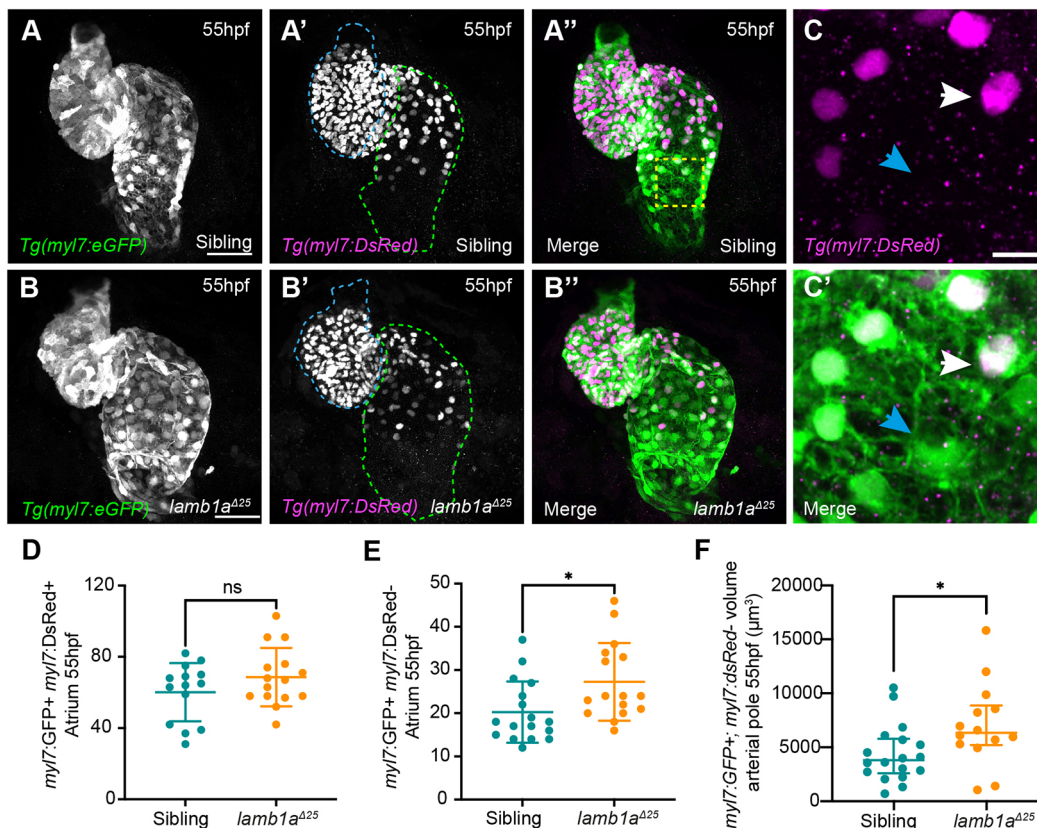


Fig. 4. Lamb1a limits SHF addition to the venous pole. (A-B'') Maximum intensity projections of confocal image z-stacks in *Tg(myI7:eGFP);Tg(myI7:DsRed)* double-transgenic sibling (A-A'') and *lamb1a*^{Δ25} mutant embryos (B-B'') at 55 hpf. GFP+;DsRed- SHF cells are visible at the venous (green dotted line) and arterial (blue dotted line) poles of the heart. (C,C') Higher magnification of the dashed-yellow-boxed area in A''. Double GFP+;DsRed+ cells represent 'older' cardiomyocytes (white arrow), whereas GFP+;DsRed- cells represent newly added SHF cells (blue arrowheads). (D,E) Quantification of double GFP+;DsRed+ cardiomyocytes (D) and GFP+;DsRed- SHF cells (E) in the atrium of siblings ($n=17$) and *lamb1a*^{Δ25} mutants ($n=16$) at 55 hpf reveals an increase in newly added SHF cells in *lamb1a*^{Δ25} mutants compared with siblings. Data are mean \pm s.d., analysed with the Kolmogorov-Smirnov test. (F) Quantification of GFP+;DsRed- myocardial volume in the distal arterial pole in sibling ($n=18$) and *lamb1a*^{Δ25} mutant embryos ($n=14$) at 55 hpf reveals an increase in SHF myocardium in *lamb1a*^{Δ25} mutants compared to controls. Data are median \pm interquartile range, analysed with Welch's *t*-test; * $P<0.05$, ns=not significant in all graphs. Scale bars: 10 μ m in C; 50 μ m in A,B.

studies demonstrating roles for FGF signalling in cell addition to the arterial pole (Felker et al., 2018; de Pater et al., 2009). Although the heart grows almost exclusively through SHF addition between 1 dpf and 2 dpf (de Pater et al., 2009), we wished to rule out an increase in proliferation in *lamb1a* mutants driving increased cell number. Quantification of the number of phospho-histone H3 (pH3) cells in sibling and *lamb1a^{Δ25}* mutant embryos at 55 hpf revealed no increased cell proliferation in *lamb1a^{Δ25}* mutants (Fig. S7G), further supporting the hypothesis that cardiomegaly in *lamb1a* mutants is driven by the increased addition of SHF cells.

Excessive second heart field addition to the venous pole in *lamb1a* mutants is dependent on heart contractility

The increased SHF addition to the atrium in *lamb1a* mutants without expansion of the SHF domain suggested a SHF specification-independent mechanism. Our finding that *lamb1b* upregulation in *lamb1a* mutants was not triggered by compensatory pathways and did not play a functional role (Fig. S4) may provide clues to the mechanisms underlying increased SHF addition in *lamb1a* mutants.

During heart morphogenesis and SHF addition, *lamb1b* is expressed throughout the endocardium at 30 hpf and, by 55 hpf, is restricted to the atrioventricular canal, the site of atrioventricular valve development (Fig. 1). This expression dynamic is similar to genes required for valvulogenesis, such as *notch1b* and *fibronectin 1b*, which are regulated by the sensation of blood flow (Steed et al., 2016; Vermot et al., 2009). We hypothesized that *lamb1b* expression is also flow dependent, and that the misexpression of *lamb1b* throughout the endocardium of *lamb1a^{Δ25}* mutants may reflect changes in cardiac function or sensitivity to blood flow upon loss of laminin.

To investigate this, embryos from a *lamb1a^{Δ25}* heterozygous incross were injected at the one-cell stage with a translation-blocking morpholino oligonucleotide (MO) targeting *troponin T type 2a (cardiac) (tnnt2a)* to block heart contractility and abolish blood flow (Sehnert et al., 2002). Expression of *lamb1b* was then examined at 30 hpf (Fig. 5A-F), when uninjected and control *tp53* MO-injected sibling embryos have low levels of endocardial *lamb1b* expression (Fig. 5A,B), and uninjected and control-injected *lamb1a^{Δ25}* mutants misexpress *lamb1b* throughout the endocardium (Fig. 5D,E). As expected, MO-mediated knockdown of *tnnt2a* in sibling embryos resulted in a loss of *lamb1b* expression in the endocardium (Fig. 5C). Similarly, loss of heart contractility in *lamb1a^{Δ25}* mutants resulted in reduced endocardial expression of *lamb1b* compared with control mutants (Fig. 5F). Together, these results demonstrate that endocardial expansion of *lamb1b* in *lamb1a^{Δ25}* mutants is dependent on heart contractility.

To confirm altered flow responsiveness in *lamb1a^{Δ25}* mutant endocardium, we analysed expression of *klf2a*, a transcription factor the expression of which is regulated by turbulent flow (Vermot et al., 2009). We injected embryos from a *lamb1a^{Δ25}* heterozygous incross with *tnnt2a* MO and examined *klf2a* expression at 30 hpf. In sibling uninjected and control embryos, *klf2a* expression was localised predominantly to the arterial pole endocardium (Fig. 5G, H), whereas uninjected and control-injected *lamb1a* mutants misexpressed *klf2a* more broadly throughout the heart (Fig. 5J,K). MO-mediated knockdown of *tnnt2a* in sibling embryos resulted in almost total loss of *klf2a* expression in the endocardium compared with controls (Fig. 5I). Similar to the effect on *lamb1b* expression, loss of heart contractility in *lamb1a^{Δ25}* mutants resulted in reduced endocardial expression of *klf2a* compared with control mutants (Fig. 5L). Together, these data suggest that loss of *Lamb1a* results in

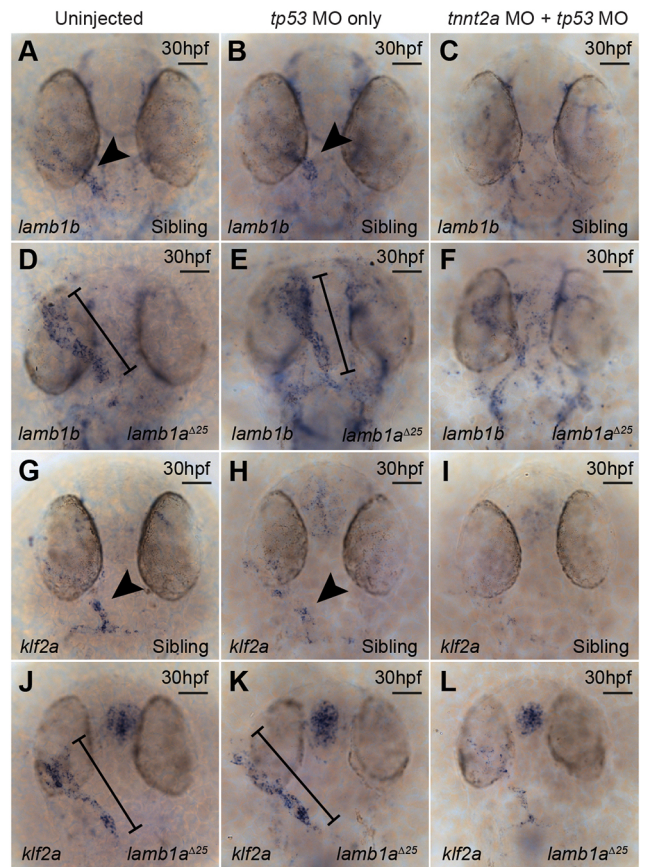


Fig. 5. *lamb1a* mutants exhibit aberrant turbulent flow sensing.

(A-F) mRNA *in situ* hybridisation analysis of *lamb1b* expression at 30 hpf in sibling (A-C) and *lamb1a^{Δ25}* mutant embryos (D-F), either uninjected (A,D), injected with a *tp53* MO (B,E) or injected with a *tp53* MO+*tnnt2a* MO (C,F). *lamb1b* is expressed predominantly in the ventricle/arterial pole of the heart tube endocardium in sibling uninjected ($n=39/45$) and control *tp53* MO-injected embryos ($n=43/46$) at 30 hpf (arrowheads in A,B), but is lost in embryos injected with *tnnt2a* MO (C; $n=35/40$). *lamb1b* expression is upregulated throughout the endocardium in uninjected ($n=23/23$) and control *tp53* MO-injected *lamb1a^{Δ25}* mutants ($n=24/28$) at 30 hpf (black lines; D,E) compared with sibling controls (arrowheads in A,B). Endocardial *lamb1b* expression is reduced in *lamb1a^{Δ25}* mutants injected with *tnnt2a* MO (F; $n=24/28$) compared with control *lamb1a^{Δ25}* mutants (D,E). (G-L) mRNA *in situ* hybridisation analysis of *klf2a* expression at 30 hpf in siblings (G-I) and *lamb1a^{Δ25}* mutants (J-L), either uninjected (G,J), injected with a *tp53* MO (H,I) or with a *tp53* MO+*tnnt2a* MO (I,L). *klf2a* is expressed at low levels throughout the endocardium, with elevated expression at the arterial pole in sibling uninjected ($n=42/43$) and control *tp53* MO-injected ($n=37/39$) embryos at 30 hpf (arrowheads in G,H), but is lost in embryos injected with *tnnt2a* MO (I; $n=31/49$). *klf2a* expression is upregulated particularly at the venous pole and atrium of *lamb1a^{Δ25}* uninjected ($n=23/25$) and control *tp53* MO-injected mutant embryos ($n=18/18$) at 30 hpf (black lines; J,K) compared with sibling controls (arrowheads in G,H). Endocardial *klf2a* expression is reduced in *lamb1a^{Δ25}* mutants injected with *tnnt2a* MO (L; $n=20/22$) compared with control *lamb1a^{Δ25}* mutants (J,K). Scale bars: 50 μ m.

perturbations to the response to heart contractility and/or blood flow during heart looping morphogenesis.

The increase in SHF addition and altered expression of haemodynamic-responsive genes suggest that cardiac function may play a role in the failure to restrict heart size in *lamb1a* mutants. We investigated whether perturbing contractile and/or haemodynamic forces rescued cardiomegaly in *lamb1a^{Δ25}* mutants by injecting the *tnnt2a* MO and measuring heart size (Fig. 6A-D). Blocking cardiac contractility in *lamb1a^{Δ25}* mutant embryos

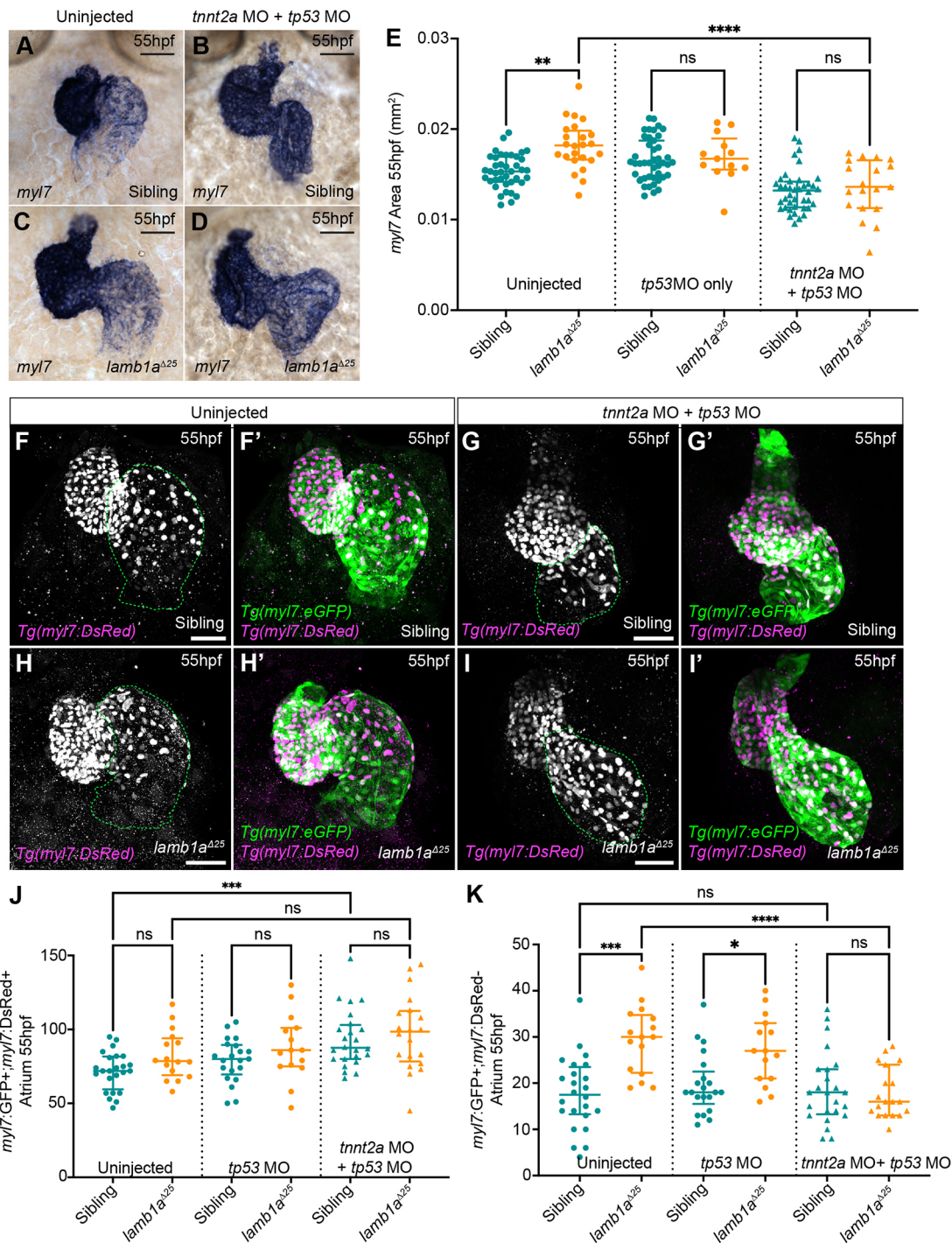


Fig. 6. Lamb1a limits excessive, contractility-dependent SHF addition to the venous pole. (A–D) mRNA *in situ* hybridisation analysis of *myl7* expression in sibling (A,B) and *lamb1a*^{Δ25} mutant embryos (C,D) either uninjected (A,C) or injected with *tp53* MO+*tnnt2a* MO (B,D). (E) Quantification of *myl7* area in uninjected (sibling: *n*=40; *lamb1a*^{Δ25}: *n*=24), *tp53* MO-injected control (sibling: *n*=43; *lamb1a*^{Δ25}: *n*=13) and *tp53* MO+*tnnt2a* MO-injected (sibling: *n*=40; *lamb1a*^{Δ25}: *n*=19) embryos at 55 hpf. Data are median±interquartile range, analysed with the Kruskal–Wallis test with multiple comparisons. (F–I') Maximum intensity projections of confocal image z-stacks in *Tg(myI7:eGFP);Tg(myI7:DsRed)* double-transgenic sibling (F–G') and *lamb1a*^{Δ25} mutant embryos (H–I') at 55 hpf, either uninjected (F,F',H,H') or injected with *tp53* MO+*tnnt2a* MO (G,G',I,I'). Green dotted lines indicate the atrium. (J,K) Quantification of double GFP+;DsRed+ atrial cardiomyocytes (J) and GFP+;DsRed– SHF cells (K) at 55 hpf in siblings and *lamb1a* mutants either uninjected (sibling: *n*=24; *lamb1a*^{Δ25}: *n*=16), injected with *tp53* MO (sibling: *n*=21; *lamb1a*^{Δ25}: *n*=15) or injected with *tp53* MO+*tnnt2a* MO (sibling: *n*=24; *lamb1a*^{Δ25}: *n*=20). Blocking heart contractility with the *tnnt2a* MO rescues excess SHF addition in *lamb1a* mutants (K). Data are median±interquartile range, analysed with Brown–Forsythe and Welch ANOVAs with multiple comparisons; *****P*<0.0001, ****P*<0.001, ***P*<0.01, **P*<0.05, ns=not significant in all graphs. Scale bars: 50 μm.

significantly reduced heart size at 55 hpf and 72 hpf compared with control *lamb1a*^{Δ25} mutants, suggesting that excess SHF addition is mediated by contractility upon loss of *lamb1a* (Fig. 6E; Fig. S8A).

To confirm this, we examined the impact of loss of heart contractility specifically on SHF addition to the venous pole of the heart at 55 hpf in *Tg(myI7:eGFP);Tg(myI7:DsRed)* transgenic

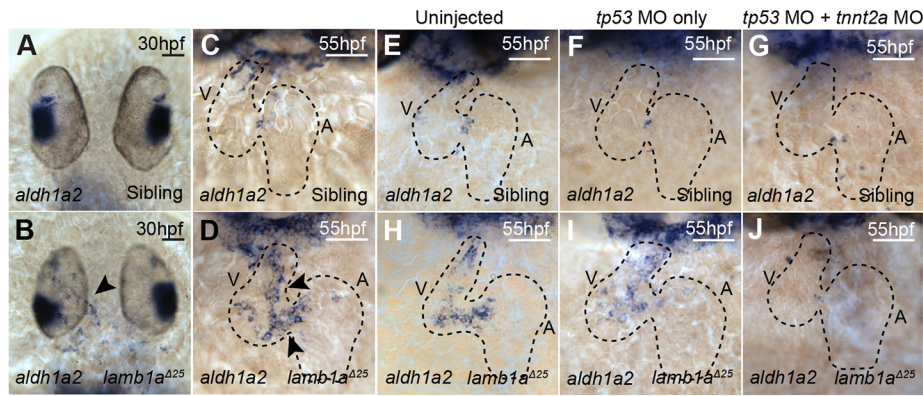


Fig. 7. *aldh1a2* upregulation in *lamb1a* mutants is contractility dependent. (A–D) mRNA *in situ* hybridisation analysis of *aldh1a2* expression in sibling and *lamb1a*^{A25} mutant embryos at 30 hpf (A,B) and 55 hpf (C,D). *lamb1a*^{A25} mutants exhibit an upregulation of *aldh1a2* expression in the endocardium at both stages (arrowheads in B,D; 30 hpf: *n*=14/20; 55 hpf: *n*=16/17) compared with siblings (30 hpf: *n*=65/66; 55 hpf: *n*=48/53). (E–J) mRNA *in situ* hybridisation analysis of *aldh1a2* expression at 55 hpf in sibling and *lamb1a*^{A25} mutant embryos, either uninjected (E,H), injected with *tp53* MO (F,I) or co-injected with *tp53* MO and *tnnt2a* MO (G,J). The upregulation of *aldh1a2* expression in the endocardium of *lamb1a*^{A25} mutants (H: *n*=12/14; I: *n*=12/16) is lost upon injection with *tnnt2a* MO (J: *n*=12/18). Black-dashed outlines indicate the heart. Scale bars: 50 µm. A, atrium; V, ventricle.

embryos (Fig. 6F–I'). In line with our previous data, uninjected and control-injected *lamb1a*^{A25} mutant embryos displayed an increase in the number of newly added SHF cells in the atrium at 55 hpf (Fig. 6K). However, in *lamb1a*^{A25} mutants injected with *tnnt2a* MO, addition of SHF cells to the atrium was rescued to levels comparable with siblings (Fig. 6K). Surprisingly, we also observed that loss of heart contractility in sibling embryos resulted in a subtle, yet significant, increase in GFP+;DsRed+ cells in the atrium at 55 hpf (Fig. 6J). This suggests more broadly that heart contractility may limit the timing of SHF addition to the atrium. Taken together, these data demonstrate that *Lamb1a* is required to limit excessive, contractile-dependent SHF addition to the atrium during heart looping morphogenesis.

To further investigate the interaction between loss of *lamb1a* and heart function, we analysed heart rate in *lamb1a* mutants. Heart rate at 2 dpf and 3 dpf was not significantly different between sibling and *lamb1a*^{A25} mutant embryos (Fig. S8B), suggesting that increased rate of heart contractility is not driving aberrant, contractility-mediated SHF addition. Additionally, having observed changes in the expression of flow-responsive genes in *lamb1a*^{A25} mutant embryos, we examined the role of shear stress in the generation of cardiomegaly in *lamb1a* mutants. We reduced blood viscosity by injecting embryos from an incross of *lamb1a*^{A25} heterozygous adults with a MO targeting the transcription factor *gata1a*, a master regulator of erythropoiesis (Brownlie and Zon, 1999; Hsu et al., 2019). Knockdown efficiency was confirmed by expression analysis of the haemoglobin subunit *hemoglobin beta embryonic-1.1* (*hbbe1.1*) (Quinkertz and Campos-Ortega, 1999) in control and *gata1a*-injected embryos at 55 hpf (Fig. S8C–E), and heart morphology was analysed at 72 hpf by *myl7* expression. Quantification of heart area revealed that loss of *Gata1a* function and the resulting reduction in blood viscosity did not rescue *lamb1a*^{A25} mutant heart size (Fig. S8F). Therefore, these data demonstrate that loss of *lamb1a* results in excessive SHF addition to the atrium through a contractile-dependent, shear stress-independent mechanism.

Retinoic acid treatment during early SHF addition partially rescues cardiomegaly in *lamb1a* mutants

The molecular pathways underlying SHF patterning and addition are conserved among vertebrates. Complex, antagonistic, FGF8 and RA signalling networks act across the atrioventricular axis of the

cardiac-forming region (Rochais et al., 2009). We showed an increase in atrial cell number and volume of SHF-derived tissue at the arterial pole, which correlated with a mild upregulation of the FGF-response gene *spry4* in the ventricle of *lamb1a* mutants at 55 hpf (Fig. S7E,F). Given that cardiac function has been implicated in regulating the expression of *aldh1a2* (formerly *raldh2*), a key enzyme in the RA synthetic pathway (Morton et al., 2008), we examined *aldh1a2* (involved in RA synthesis and a RA-signalling target) expression in *lamb1a*^{A25} mutants (Fig. 7). At 30 hpf, *lamb1a*^{A25} mutants exhibited a marked upregulation of *aldh1a2* expression throughout the endocardium, including in the venous pole/atrium (Fig. 7A,B), similar to the upregulated expression of *lamb1b* and *klf2a* (Fig. 5). This upregulation persisted at 55 hpf in the ventricle of *lamb1a* mutants (Fig. 7C,D), similar to the upregulation of *lamb1b* (Fig. S4). Therefore, to investigate whether the impact of loss of *lamb1a* on RA signalling is also contractility dependent, we examined *aldh1a2* expression in sibling and *lamb1a*^{A25} mutant embryos injected with *tnnt2a* MO. Whereas uninjected and control injected *lamb1a*^{A25} mutant embryos had a clear expansion of *aldh1a2* (Fig. 7H,I), MO-mediated knockdown of *tnnt2a* abrogated endocardial *aldh1a2* expression in *lamb1a*^{A25} mutants (Fig. 7J). Together, these results suggest not only that disruption to RA signalling in *lamb1a*^{A25} mutants is partly regulated by heart function, but also that cardiac contractility itself influences activity of the pathways regulating SHF addition.

Having established that excessive SHF addition in *lamb1a* mutants is dependent on heart contractility, and that RA signalling appears dysregulated upon loss of laminin in a contractility-dependent manner, we investigated whether we could rescue cardiomegaly in *lamb1a* mutants through modulation of RA. Studies in mouse have shown that loss of RA signalling in *aldh1a2* mutants results in hypoplastic atria (Niederreither et al., 2001; Sirbu et al., 2008), that upregulation of *aldh1a2* is a consequence of insufficient RA signalling (Chen et al., 2001; Dobbs-McAuliffe et al., 2004; Niederreither et al., 1997), and that increased *spry4* expression suggests overactive FGF signalling, which is antagonised by RA signalling (Rochais et al., 2009). Therefore, we hypothesised that addition of exogenous RA during early heart looping morphogenesis may rescue heart size in *lamb1a* mutants. We treated embryos from a *lamb1a*^{A25} heterozygous incross from 24 hpf to 55 hpf with 100 nM RA, washed the drug off

and allowed the embryos to develop to 72 hpf. We confirmed the efficacy of our drug treatment by expression analysis of the RA-responsive gene *dhrs3a* (Waxman et al., 2008), which was upregulated at 55 hpf upon RA treatment (Fig. S9A-F). Analysis of heart size in sibling and *lamb1a*^{A25} mutant embryos at 72 hpf following 100 nM RA treatment revealed only a partial rescue of cardiac size in *lamb1a* mutants (Fig. S9G-P). This suggests that, although contractility-dependent RA signalling in *lamb1a* mutants is perturbed, this is not the only pathway driving increased heart size, and that heart function likely affects SHF addition through additional mechanisms.

Thus, we have shown for the first time the requirement for laminins in regulating early vertebrate heart morphogenesis, promoting heart morphology and restricting heart size through restriction of SHF addition. Furthermore, our data suggest that the ECM and cardiac contractility function together to regulate the balance of SHF-related signalling pathways.

DISCUSSION

We provide the first evidence that laminin restricts heart growth during looping morphogenesis by limiting the number of SHF cells incorporated into the venous pole of the heart. Previous studies identified roles for ECM components, such as versican and fibronectin (Fn), in promoting SHF addition to the arterial pole of the heart (Kern et al., 2007; Mittal et al., 2013, 2019; Mjaatvedt et al., 1998; Yamamura et al., 1997); however, we identified an opposing role for Lamb1a in restricting excessive SHF addition to both poles. Highlighting the importance of cell-ECM interactions in the SHF, loss of *Tbx1*, a master regulator of SHF addition, results in reduced expression of integrin, loss of focal adhesion markers, and impaired filopodia formation in the SHF (Alfano et al., 2019; Francou et al., 2014).

Heart function is tightly linked to heart morphology during development, and previous studies focussed on the impact of contraction on regionalised ventricular cell shape change, valvulogenesis and trabeculation (Auman et al., 2007; Bartman et al., 2004; Cai et al., 2019; Samsa et al., 2015; Staudt et al., 2014). Our finding that excessive atrial SHF addition in *lamb1a* mutants can be rescued by abolishing heart contractility (Fig. 6) suggests that laminin may alter the physical force of heart contractility. *lamb1a* and *lamc1* are expressed broadly throughout the zebrafish embryo during the window of SHF migration, both within the heart and in the surrounding tissues in which the SHF resides. Therefore, whether the role of Lamb1a in restricting SHF addition is autonomous or non-autonomous to the heart tube remains an open question.

The upregulation of flow-sensitive *klf2a* expression in *lamb1a* mutants suggests that the dynamics of myocardial wall contraction may be altered. Given that laminins coordinate ECM assembly, loss of laminin may alter ECM stiffness, which has been shown *in vitro* to impact cardiomyocyte contractility (Bhana et al., 2010; Engler et al., 2008), whereas ECM composition can also affect the organisation of contractile apparatus in cardiomyocytes (Bildjug and Pinaev, 2014; Hilenski et al., 1989; Vanwinkle et al., 1996). Alternatively, loss of laminin could affect how SHF cells interact with the underlying ECM. Studies in mouse have shown that epithelial tension in the posterior SHF is accompanied by nuclear localisation of the mechanosensitive transcription factor YAP (Francou et al., 2017), a phenomenon associated with increased ECM stiffness (Dobrokhotoev et al., 2018), and recent *in vitro* studies demonstrated that laminin itself promotes nuclear YAP shuttling in keratinocytes (De Rosa et al., 2019). Activation of YAP/TAZ signalling in the SHF at the venous pole of the heart is conserved in

zebrafish (Fukui et al., 2018), and the increased atrial SHF addition in 55 hpf in *lamb1a* mutants is similar to that observed in *lats1/lats2* double mutants, which have a global increase in activity of YAP/TAZ signalling (Fukui et al., 2018). This suggests that ECM-mediated mechanotransduction in the SHF may represent a conserved mechanism regulating SHF addition that is disrupted in *lamb1a* mutants. How this is impacted by cardiac contraction is unclear, although it has been speculated that cardiac function could contribute to SHF tension (Francou et al., 2017), and it is conceivable that cardiomyocyte contractility contributes to the balance of pulling and pushing forces regulating SHF incorporation into the OFT in mice (Li et al., 2016). Mechanical loading has been implicated as a moderator of ECM content in other contexts, such as bone (Humphrey et al., 2014). Therefore, it is possible that loss of heart contractility could affect the composition of the cardiac ECM by, for example, upregulating ECM components, which could restore a suitable environment for SHF addition in *lamb1a* mutants. Importantly, although blocking contractility rescued excessive cell addition to the venous pole in *lamb1a* mutants, morphology of the inflow tract appeared impaired (Fig. 6), suggesting that cardiac contraction is also required to shape the venous pole.

In addition to facilitating cell-ECM interactions, laminins are crucial for ECM assembly, interacting with ECM components such as heparan sulfate proteoglycans (HSPGs). In turn, HSPGs interact with additional ECM components, such as Fn, and signalling molecules, such as FGF (Mouw et al., 2014). HSPG and Fn both regulate FGF signalling during SHF addition to the OFT/arterial pole in mice (Mittal et al., 2010; Zhang et al., 2015); therefore, laminin may interact with HSPGs to regulate extracellular signalling promoting SHF addition. Supporting this, we observed a mild upregulation of the FGF-response gene *spry4* in the ventricle of *lamb1a* mutant hearts at 55 hpf (Fig. S7). However, levels of FGF activity are also balanced by antagonistic RA signalling, and the upregulation of the RA-responsive RA-synthesising enzyme *aldh1a2* in *lamb1a* mutants (Fig. 7) suggests that RA signalling is impaired, leading to a dysregulation of FGF activity. Supporting this hypothesis, timed RA treatments during early SHF addition partially rescued heart size in *lamb1a* mutants at 3 dpf (Fig. S9). However, global upregulation of RA is likely too broad to restore the balance of RA-FGF levels, and, therefore, it is difficult to interpret the specific contribution of disrupted RA signalling to the increased SHF addition and cardiomegaly in *lamb1a* mutants, given the complex antagonistic interactions. RA signalling during early development was recently proposed to define the rate of cardiac progenitor differentiation in the anterior lateral plate mesoderm, because disruption of RA signalling from 6 hpf onwards results in a reduction in *ltp3* expression and a loss of *isl1a*-positive pacemaker cells at the inflow tract (Duong et al., 2021). Importantly, we did not observe changes in the size of the *isl1a* expression domains at the venous pole (Fig. S7), suggesting that altered FGF-RA signalling does not affect the size of the SHF progenitor populations in *lamb1a* mutants and that RA signalling is disrupted after SHF specification. Furthermore, analysis of *aldh1a2* expression in *lamb1a* mutants in which cardiac contractility had been abrogated revealed that *aldh1a2* upregulation in *lamb1a* mutants is dependent on heart function. This suggests that dysregulation of RA signalling is secondary to altered contractility in *lamb1a* mutants, highlighting the complexity of interaction between the ECM, cardiac function, cell signalling, and SHF addition. Our observation that the size of the *isl1a* expression domain was not increased in *lamb1a* mutants, coupled with our finding that proliferation was not upregulated at 55 hpf, supports the requirement for *lamb1a* in specifically

regulating the timing or rate at which SHF cells are added to the venous pole. Although we suggest that this addition alone is sufficient to drive the increase in atrial size observed in *lamb1a* mutants, it is possible that SHF cells exhibit a transient increase in proliferation after they have been added to the heart or there is a subtle increase in the proliferative index of the myocardium, which we were unable to capture in this study.

Both *LAMB1* and *LAMB2* are detectable in human heart samples at gestational weeks 8/9, and are deposited into the ECM that surrounds the cardiomyocytes and the basement membrane of the endocardium (Roediger et al., 2010). Mutations in *LAMC1* are linked with DWS, a rare CNS disorder associated with congenital heart defects (Darbro et al., 2013). We showed a conserved requirement for zebrafish *lamc1* in heart morphogenesis, with crispants also displaying hydrocephalus (Fig. 2; Fig. S2), another symptom associated with DWS. Furthermore, our finding that loss of laminin may lead to altered contractility and heart morphology at relatively early stages of cardiac development could shed further light on the mechanisms underlying the progression of dilated cardiomyopathy in individuals with *LAMA4* mutations (Knöll et al., 2007), given that contractile dysfunction is a factor in the initiation of cardiac remodelling and cardiomyopathies (Vikhorev and Vikhoreva, 2018). This conservation of laminin function highlights the value of zebrafish as a model for understanding the role of ECM dysfunction in human cardiac diseases.

Thus, we describe the first direct evidence that laminins promote morphogenesis and growth during early vertebrate heart development, uncovering a novel role for laminin in restricting contractility-dependent SHF addition to the venous pole. This work also identifies new links between ECM composition, mechanical and biochemical cues in shaping the heart, reinforcing the importance of the extracellular environment during organ morphogenesis.

MATERIALS AND METHODS

Zebrafish maintenance

Adult zebrafish (*D. rerio*) were maintained according to standard laboratory conditions. The following, previously described lines were used: WT (AB), *Tg(myl7:eGFP)* (Huang et al., 2003), *Tg(myl7:lifeActGFP)* (Reischauer et al., 2014), *Tg(-5.1myl7:DsRed2-NLS)²* (Rottbauer et al., 2002), *grumpy^{jl299a}* (Odenthal et al., 1996) and *sleepy^{sa379}* (Kettleborough et al., 2013). The lines generated for this study were: *lamb1a^{Δ19}* (*lamb1a^{sh589}*), *lamb1a^{Δ25}* (*lamb1a^{sh590}*), *lamb1b^{promΔ183}* (*lamb1b^{sh587}*) and *lamb1b^{promΔ428}* (*lamb1b^{sh588}*). Embryos were maintained in E3 medium (5 mM NaCl, 0.17 mM KCl, 0.33 mM CaCl₂, 0.33 mM MgSO₄) at 28.5°C and were staged according to Kimmel et al. (1995). Embryos older than 24 hpf were transferred into E3 medium containing 0.003% 1-phenyl 2-thiourea (PTU, Sigma-Aldrich P7629) to inhibit pigment formation and aid imaging. Animal work was approved by the local Animal Welfare and Ethical Review Body (AWERB) at the University of Sheffield, conducted in accordance with UK Home Office Regulations under PPLs 70/8588 and PA1C7120E, and in line with the guidelines from Directive 2010/63/EU of the European Parliament on the protection of animals used for scientific purposes.

Generation of *lamb1a* mutants

To generate *lamb1a* (ENSDART00000170673.2) mutant zebrafish, *lamb1a*-targeting gRNAs were designed using CHOPCHOP (Labun et al., 2016; Montague et al., 2014) and, following selection of suitable gene-specific sequences, the first two nucleotides were converted from NG/GN to GG and the PAM sequence (NGG) was removed. A single gRNA targeting exon 6 (5'-GGATCCTCAATCCTGAAGGCAGG-3') was selected. The reverse complement of the resulting sequence was inserted into an ultramer scaffold sequence (Hruscha et al., 2013) containing a T7

promoter (AAAGCACCGACTCGGTGCCACTTTTCAAGTTGATAACGGACTAGCCTTATTTAACTTGCTATTTCTAGCTCTAAAACxxxx-xxxxxxxxxxxxxxxxCTATAGTGAGTCGTATTACGC), where 'x' denotes insertion site for gene-specific targeting sequence. The template was amplified by PCR (F: 5'-GCGTAATACGACTCACTATAG-3', R: 5'-AAAGCACCGACTCGGTGCCAC-3') and used as a template for *in vitro* transcription using MEGAshortscript T7 kit (Ambion/Thermo Fisher Scientific AM1354). gRNA was injected together with Cas9 protein (New England Biolabs M0386T) and Phenol Red (Sigma-Aldrich P0290) into the yolk at the one-cell stage. Each embryo was injected with 2 ng gRNA, 1.9 nM Cas9 protein and 10% Phenol Red. CRISPR Cas9-injected embryos were raised to adulthood (F0) and outcrossed to WT to identify F0 individuals with germline transmission of deletions that result in a frameshift and subsequent premature termination codon. Embryos from F0 outcrosses were genotyped by PCR to amplify the region of *lamb1a* targeted for mutagenesis (F: 5'-CTTCTGTCTCTCATGGGCCA-3', R: 5'-TGCCTTACTTTGAATTCTGGGG-3'), and mutations were analysed by Sanger sequencing. Two *lamb1a*-coding sequence deletion alleles were recovered: *lamb1a^{Δ19}* (*lamb1a^{sh589}*) and *lamb1a^{Δ25}* (*lamb1a^{sh590}*). F0 founders transmitting these mutations were outcrossed to WT (AB) and offspring were raised to adulthood. Phenotypic analyses were carried out using F2 or F3 adults.

Generation of *lamb1b* promoter mutants

Two gRNAs were designed to target the upstream of the annotated promoter of *lamb1b* (ENSDARG00000045524) according to the Eukaryotic Promoter Database (Dreos et al., 2015, 2017) [*lamb1b* CRISPR RNA (crRNA) 1: 5'-TTGTTAATAGCATAGTACATTGG-3'; underlining denotes the protospacer adjacent motif (PAM)] and downstream of the annotated initiation codon (*lamb1b* crRNA 2: 5'-GGAGAACAAGCAAACGATGAGG-3'; underlining denotes the PAM). Sequence-specific crRNAs were synthesised by Merck, resuspended in MilliQ (MerckMillipore) water to 500 μM and dilutions made for working stocks. Next, 2 nl of a Cas9-gRNA ribonucleoprotein complex was injected into the yolk of one-cell-stage embryos. Each embryo was injected with 61.2 nM crRNA, 122.5 nM tracrRNA, 3.9 nM Cas9 and 14% Phenol Red.

CRISPR Cas9-injected embryos were raised to adulthood (F0) and individual adults were outcrossed to WT to identify the germline transmission of suitable promoter deletions. Embryos collected from these outcrosses were genotyped by PCR to amplify the region of *lamb1b* targeted for mutagenesis (Forward: 5'-TCACACTAAGACATGGGGCA-3', Reverse: 5'-ACCAAGCAACAAAACACTGA-3'). Successful promoter deletion was identified by the presence of a smaller PCR fragment by gel electrophoresis and subsequent Sanger sequencing of the PCR fragment to confirm the deletion. Two separate *lamb1b* promoter deletion alleles were recovered: *lamb1b^{promΔ183}* (*lamb1b^{sh587}*) and *lamb1b^{promΔ428}* (*lamb1b^{sh588}*). F0 founders transmitting these mutations were outcrossed to *lamb1a^{Δ25}* heterozygous adults and offspring were raised to adulthood. Heterozygous F1 *lamb1a*; *lamb1b* adults were genotyped using the relevant primers for each locus and used for experiments.

CRISPR-Cas9-mediated *lamc1* and *lamb2* F0 mutagenesis

lamc1 and *lamb2* F0 CRISPR mutagenesis was carried out as previously described (Burger et al., 2016; Wu et al., 2018). *lamc1*- and *lamb2*-targeting gRNAs were designed using CHOPCHOP. gRNAs were synthesised following the method described for *lamb1a* mutagenesis. gRNAs were designed to target the initiation codon of *lamc1* (ENSDART00000004277.8) (*lamc1* F0 gRNA1: 5'-GGCTTCAATGCGACCGTGGTGG-3'; *lamc1* F0 gRNA2: 5'-GGCGTGCAGTCACG-GAGCGATGG-3'). gRNAs were designed to target exons 6, 12, 20 and 24 of *lamb2* (ENSDART00000147326.2) (*lamb2* F0 gRNA1: 5'-GGA-CAGTGTCCATGCCGACCTGG-3'; *lamb2* F0 gRNA2: 5'-CGAGCCGTCGACAGAGGAGGAGG-3'; *lamb2* F0 gRNA3: 5'-TGCCGAAACTGTACCCCTGGGG-3'; *lamb2* F0 gRNA4: 5'-AGACTGTCAGGAGAACCCTGGG-3'). The injection mix containing gRNA, Cas9 protein and Phenol Red was assembled on ice and incubated at 37°C for 5 min to aid Cas9-gRNA ribonucleoprotein complex formation for more efficient mutagenesis, prior to loading into a microinjection needle.

Then, 1 nl of Cas9-gRNA was injected into the yolk of one-cell-stage embryos; each injection comprised either 500 pg of each gRNA for *lamc1* or 214.3 pg of each gRNA for *lamb2*, in addition to 1.9 nM Cas9 protein and 14% Phenol Red. Mutagenesis was confirmed through PCR amplification of the targeted region of genomic DNA (*lamc1* Forward: 5-ATCAAGA-CAGTGACGGTAGCAA-3', Reverse: 5'-TGTGGCATGATTTAGTG-ACTCC-3'; *lamb2* target 1 Forward: 5'-TGTGAATGCAGTTTLAGAG-GGCT-3', Reverse: 5'-CAGCACACTCTCTGATTTTTGC-3'; *lamb2* target 2 Forward: 5'-CTGGCAGGTATCGCTACTTT-3', Reverse: 5'-ATCCTGATAGCAGGGTCAAGAA-3'; *lamb2* target 3 Forward: 5'-ACC-TCTGCACTTTTAGACCACC-3', Reverse: 5'-TAACCAAATGTTCTCA-GAGGGG-3'; *lamb2* target 4 Forward: 5'-CATACAGTTTACAGGC-CAGTGC-3', Reverse: 5'-GGGAGAGAATCAAACCAGAAAA-3'); uninjected, gRNA-only injected and Cas9-only injected embryos were included as controls. Multiple lesions induced by CRISPR-mediated mutagenesis resulted in heteroduplex formation during PCR, which were resolved on a 4% agarose TBE gel. For initial experiments, mutagenesis was confirmed by Sanger sequencing of heteroduplex PCR products, and multiple lesions were identified at the target site. *lamc1* mutagenesis was confirmed through heteroduplex analysis of the target loci in embryos displaying a morphological *lamc1* mutant phenotype. Given that *lamb2* mutants do not exhibit characteristic defects in overt morphology, efficacy was determined via heteroduplex analysis for all four *lamb2* guides (gRNA1: 88%, $n=30$; gRNA2: 90%, $n=20$; gRNA3: 88%, $n=30$; gRNA4: 88%, $n=30$). However, in instances when mutagenesis was not observed at one gRNA target site, lesions were not observed at any of the four target sites in the same embryo, suggesting that the microinjection itself in those embryos was unsuccessful. Given that all four guides induced lesions in almost all injected embryos, successful mutagenesis by gRNA4 was used to genotype all subsequent experiments (efficacy=86%, $n=137$) and embryos in which lesions were not identified were discarded from analysis. Uninjected and gRNA-only injected controls were included in all heteroduplex analyses.

Morpholino-mediated knockdown

All MOs used are previously described: *tp53*-MO (Langheinrich et al., 2002), *tmt2a*-MO (Sehnert et al., 2002) and *gata1a*-MO (Galloway et al., 2005). *tp53* and *tmt2a* MOs were purchased from GeneTools and resuspended in MilliQ to 1 mM. The following concentrations were used for knockdown: *tp53* 250 nM and *tmt2a* 125 nM. The *gata1a* MO was a gift from J. Serbanovic-Canic (University of Sheffield, UK), and injected at 200 nM. *tmt2a* or *gata1a* MOs were co-injected with the *tp53* MO. Embryos were injected with 1 nl of MO solution into the yolk at the one-cell stage.

mRNA *in situ* hybridisation

For chromogenic mRNA *in situ* hybridisation, embryos were fixed overnight in 4% paraformaldehyde (PFA, Cell Signalling Technology 12606); for fluorescence mRNA *in situ* hybridisation, embryos were fixed overnight in 4% PFA containing 4% sucrose. Following fixation, embryos were washed three times for 5 min each in PBS-Tween [PBST; 0.2% Tween (Sigma-Aldrich P2287) in PBS (Thermo-Fisher Scientific BR0014G)] and transferred into 100% MeOH for storage at -20°C . Chromogenic mRNA *in situ* hybridisation was carried out as previously described (Noël et al., 2013). Fluorescence *in situ* hybridisations were carried out using the PerkinElmer TSA kit (Welten et al., 2006). The fluorescence-labelled *fli1* riboprobe was developed with Tyr-Cy5 (PerkinElmer NEL705A001KT), followed by the digoxigenin (DIG)-labelled gene of interest riboprobe developed with Tyr-Cy3 (PerkinElmer NEL704A001KT). Following probe signal amplification, embryos were fixed in 4% PFA with sucrose overnight and then washed into PBST for immunohistochemistry. The following previously published probes were used: *lamb1b* (Sztal et al., 2011), *fli1* (Brown et al., 2000), *myl7* (Yelon et al., 1999), *myh6* (Derrick et al., 2021), *myh7l* (Derrick et al., 2021), *aldh1a2* (Begemann and Meyer, 2001), *spry4* (Fürthauer et al., 2001), *ltbp3* (Zhou et al., 2011), *klf2a* (Novodvorsky et al., 2015) and *hbbe1.1* (Quinkertz and Campos-Ortega, 1999). All other probes were generated for this study. Probe constructs were generated through PCR amplification of a DNA fragment from total zebrafish cDNA at 55 hpf, and ligated into either the

pCRII-TOPO vector or pCR4-TOPO vector (Thermo Fisher Scientific 450640 and 450071). See Table S1 for probe primer and sequence details. Riboprobes were transcribed from a linearized template in the presence of DIG-11-UTP or Fluorescein-11-UTP (Roche).

Immunohistochemistry

Embryos were fixed overnight in 4% PFA containing 4% sucrose, washed three times for 5 min each in PBST and transferred into 100% MeOH for storage at -20°C . Embryos were rehydrated into PBST, washed briefly in PBST and twice for 5 min each in 0.2% Triton-X (Sigma-Aldrich T8787) in PBS (PBS-Triton). Embryos were incubated in blocking buffer [10% goat serum (Invitrogen 10000C) in PBS-Triton] at room temperature with gentle agitation for 1 h. Blocking buffer was removed and replaced with blocking buffer containing 1% DMSO and primary antibodies. Embryos were incubated overnight at 4°C with gentle agitation. Following removal of primary antibodies, embryos were extensively washed in PBS-Triton and incubated in blocking buffer containing 1% DMSO and secondary antibodies overnight at 4°C with gentle agitation. After removal of secondary antibodies, embryos were extensively washed in PBS-Triton at room temperature before being prepared for imaging. The following antibodies were used: chicken anti-GFP (1:500, Aves Labs GFP-1010), rabbit anti-DsRed (1:200, Takara Bio 632496), rabbit anti-PH3 (1:200, MerckMillipore 04-817), donkey anti-chicken-Cy2 (1:200, Jackson Immuno Research 703-225-155) and goat anti-rabbit-Cy3 (1:200, Jackson Immuno Research 111-165-003).

Retinoic acid treatments

RA powder (Sigma-Aldrich R2625-50MG) was dissolved in DMSO (Sigma-Aldrich 276855) to a stock concentration of 10 mM, and aliquots were stored at -80°C . Embryos were manually dechorionated prior to treatment, and ten *lamb1a* mutant and 13 *lamb1a* sibling embryos were placed in a glass petri dish. Stock RA was diluted 1:10,000 in E3-PTU to give a working concentration of 100 nM RA with 1% DMSO, and 8 ml was added to treatment dishes. Control embryos were incubated with either E3-PTU or E3-PTU with 1% DMSO. Embryos were incubated in RA or control medium from 24 hpf to 55 hpf, when the drug was removed by rinsing embryos three times for 5 min each in E3, and either fixed immediately or allowed to develop until 72 hpf and then fixed. Embryos were protected from light during the treatment window. Each RA treatment/control treatment was treated as one experimental unit for quantification, with an average value calculated from all embryos for each treatment. These treatment averages then formed one experimental replicate for statistical analyses, and treatments were replicated four times.

Quantification of heart rate

Prior to imaging at 2 dpf, embryos were sorted based on morphology into siblings and mutants. A pair of embryos (1 sibling, 1 mutant) was transferred in E3 medium from a 28.5°C incubator. A single embryo was positioned laterally on an agarose mould (2% agarose in E3) for imaging under a dissection microscope (11.5 \times magnification) attached to a high-speed camera (Chameleon3 USB3, FLIR Integrated Imaging Solutions) focussed on the heart. Image sequences (.tif) of 5 s were captured at 150 frames per second using SpinView Software (Spinnaker v. 2.0.0.147). This procedure was repeated for the remaining embryo of the pair and was then repeated at 3 dpf. Image sequences were imported into Fiji and converted to .avi movies. Movies were imported into, and heart rate quantified in, DanioScope (Noldus). Individual values represent an average heart rate over the 5 s imaging period.

Imaging and image quantification

Prior to quantification, files were blinded using an ImageJ Blind_Analysis plugin (modified from the Shuffler macro, v1.0 26/06/08, Christophe Leterrier, Aix-Marseille University, France). Looping ratio, heart area and chamber area were quantified as previously described (Derrick et al., 2021).

Total heart cardiomyocyte cell number and internuclear distance were quantified from *Tg(myl7:DsRed)* transgenic hearts. z -stacks of fixed hearts were imaged on a Nikon A1 confocal microscope, using a 40 \times objective with a z -resolution of 1 μm . The DsRed channel of each heart was used to

generate a depth-coded *z*-projection of the *z*-stack, using the temporal colour code function in Fiji. Cell number in the atrium and ventricle were quantified from these *z*-projections. Internuclear distance was quantified by measuring the distance between DsRed+ nuclei with the same or similar depth coding in the projection. Six cells were selected per chamber and, from each cell, the distance to the four nearest neighbours with similar *z* positions was measured. Average internuclear distance was then calculated for each chamber in each embryo.

Atrial/venous pole SHF addition was quantified similar to previous methods (de Pater et al., 2009). Stacks were opened in Fiji and converted to maximum intensity projections. Using the DsRed channel only, the intensity was increased to maximum and the number of atrial DsRed+ nuclei was quantified using the ROI Manager in Fiji; the GFP channel was used to confirm position in the heart. Using the GFP channel only, the intensity was increased to maximum and GFP+ nuclei not previously counted in the ROI Manager were quantified as DsRed-. Returning to the original stack, individual slices were examined, together with the ROIs for DsRed+ and DsRed- atrial cells to ensure that no cells had been missed or miscounted. Cells derived from the ventricle or atrioventricular canal were discounted.

Ventricular/arterial pole SHF addition was quantified by determining the amount of GFP+ tissue at the arterial pole, distal to the last DsRed+ nucleus in the ventricle/OFT. Each sample *z*-stack was reoriented in Fiji to allow transverse reslicing into the arterial pole. Once the first DsRed+ cardiomyocyte was observed, all subsequent slices were discarded and the GFP channel selected, creating a small stack representing only the GFP+ SHF-derived component of the arterial pole. The 3D Object Counter Fiji plugin was used to threshold, identify and quantify the arterial pole SHF myocardium.

Data analysis

Statistical analyses of quantitative data were performed in Graphpad Prism 9. Data were first tested for normality using the D'Agostino-Pearson test to define whether a parametric or nonparametric test was required. Mean heart size, looping ratio or cell number were compared between two samples using an unpaired *t*-test or Mann Whitney U-test, assuming unequal variance. Means were compared between multiple samples using the Brown-Forsythe and Welch ANOVA, or Kruskal-Wallis with Dunn's multiple comparisons test. Data were considered significant when $P < 0.05$.

Acknowledgements

We thank Tanya Whitfield and Juliana Sánchez-Posada for comments on the manuscript. Additional imaging work was performed at the Wolfson Light Microscopy Facility using a Nikon A1 microscope. C.J.D. would like to thank Martin and Jane Derrick for financial support during 2020.

Competing interests

The authors declare no competing or financial interests.

Author contributions

Conceptualization: C.J.D., E.S.N.; Methodology: C.J.D., E.J.G.P., E.S.N.; Validation: C.J.D., E.S.N.; Formal analysis: C.J.D., E.S.N.; Investigation: C.J.D., F.H., E.S.N.; Resources: A.S.S.U, A.J.G.; Data curation: E.S.N.; Writing - original draft: C.J.D., E.S.N.; Writing - review & editing: E.S.N.; Visualization: C.J.D., E.S.N.; Supervision: E.S.N.; Project administration: E.S.N.; Funding acquisition: E.S.N.

Funding

This work was supported by the British Heart Foundation (FS/16/37/32347 to E.S.N) and the Rosetrees Trust (M582 to C.J.D.).

Peer review history

The peer review history is available online at <https://journals.biologists.com/dev/article-lookup/doi/10.1242/dev.199691>

References

Alfano, D., Altomonte, A., Cortes, C., Bilio, M., Kelly, R. G. and Baldini, A. (2019). Tbx1 regulates extracellular matrix-cell interactions in the second heart field. *Hum. Mol. Genet.* **28**, 2295-2308. doi:10.1093/hmg/ddz058

Auman, H. J., Coleman, H., Riley, H. E., Olale, F., Tsai, H.-J. and Yelon, D. (2007). Functional modulation of cardiac form through regionally confined cell shape changes. *PLoS Biol.* **5**, e53. doi:10.1371/journal.pbio.0050053

Bartman, T., Walsh, E. C., Wen, K.-K., McKane, M., Ren, J., Alexander, J., Rubenstein, P. A. and Stainier, D. Y. R. (2004). Early myocardial function affects endocardial cushion development in zebrafish. *PLoS Biol.* **2**, e129. doi:10.1371/journal.pbio.0020129

Begemann, G. and Meyer, A. (2001). Hindbrain patterning revisited: timing and effects of retinoic acid signalling. *BioEssays* **23**, 981-986. doi:10.1002/bies.1142

Beis, D., Bartman, T., Jin, S.-W., Scott, I. C., D'Amico, L. A., Ober, E. A., Verkade, H., Frantsve, J., Field, H. A., Wehman, A. et al. (2005). Genetic and cellular analyses of zebrafish atrioventricular cushion and valve development. *Development* **132**, 4193-4204. doi:10.1242/dev.01970

Bhana, B., Iyer, R. K., Chen, W. L. K., Zhao, R., Sider, K. L., Likhithpanichkul, M., Simmons, C. A. and Radisic, M. (2010). Influence of substrate stiffness on the phenotype of heart cells. *Biotechnol. Bioeng.* **105**, 1148-1160. doi:10.1002/bit.22647

Bildjug, N. B. and Pinaev, G. P. (2014). Extracellular matrix dependence of organization of the cardiomyocyte contractile apparatus. *Cell Tissue Biol.* **8**, 38-49. doi:10.1134/S1990519X14010039

Brown, L. A., Rodaway, A. R. F., Schilling, T. F., Jowett, T., Ingham, P. W., Patient, R. K. and Sharrocks, A. D. (2000). Insights into early vasculogenesis revealed by expression of the ETS-domain transcription factor Fli-1 in wild-type and mutant zebrafish embryos. *Mech. Dev.* **90**, 237-252. doi:10.1016/S0925-4773(99)00256-7

Brownlie, A. and Zon, L. (1999). The zebrafish as a model system for the study of hematopoiesis: zebrafish mutants point the way to novel genes involved in the generation of vertebrate blood cells. *Bioscience* **49**, 382-392. doi:10.2307/1313631

Burger, A., Lindsay, H., Felker, A., Hess, C., Anders, C., Chiavacci, E., Zaugg, J., Weber, L. M., Catena, R., Jinek, M. et al. (2016). Maximizing mutagenesis with solubilized CRISPR-Cas9 ribonucleoprotein complexes. *Development* **143**, 2025-2037. doi:10.1242/dev.134809

Cai, C., Sang, C., Du, J., Jia, H., Tu, J., Wan, Q., Bao, B., Xie, S., Huang, Y., Li, A. et al. (2019). Knockout of tnn1b in zebrafish causes defects in atrioventricular valve development via the inhibition of the myocardial wnt signaling pathway. *FASEB J.* **33**, 696-710. doi:10.1096/fj.201800481RR

Chen, Y., Pollet, N., Niehrs, C. and Pieler, T. (2001). Increased XRALDH2 activity has a posteriorizing effect on the central nervous system of *Xenopus* embryos. *Mech. Dev.* **101**, 91-103. doi:10.1016/S0925-4773(00)00558-X

Darbro, B. W., Mahajan, V. B., Gakhar, L., Skeie, J. M., Campbell, E., Wu, S., Bing, X., Millen, K. J., Dobyns, W. B., Kessler, J. A. et al. (2013). Mutations in extracellular matrix genes NID1 and LAMC1 cause autosomal dominant dandy-walker malformation and occipital cephaloceles. *Hum. Mutat.* **34**, 1075-1079. doi:10.1002/humu.22351

de Pater, E., Clijsters, L., Marques, S. R., Lin, Y.-F., Garavito-Aguilar, Z. V., Yelon, D. and Bakkers, J. (2009). Distinct phases of cardiomyocyte differentiation regulate growth of the zebrafish heart. *Development* **136**, 1633-1641. doi:10.1242/dev.030924

De Rosa, L., Secone Seconetti, A., De Santis, G., Pellacani, G., Hirsch, T., Rothoef, T., Teig, N., Pellegrini, G., Bauer, J. W. and De Luca, M. (2019). Laminin 332-dependent YAP Dysregulation depletes epidermal stem cells in junctional epidermolysis bullosa. *Cell Rep.* **27**, 2036-2049.e6. doi:10.1016/j.celrep.2019.04.055

Derrick, C. J. and Noël, E. S. (2021). The ECM as a driver of heart development and repair. *Development* **148**, dev191320. doi:10.1242/dev.191320

Derrick, C. J., Sánchez-Posada, J., Hussein, F., Tessadori, F., Pollitt, E. J. G., Savage, A. M., Wilkinson, R. N., Chico, T. J., van Eeden, F. J., Bakkers, J. et al. (2021). Asymmetric Hapln1a drives regionalized cardiac ECM expansion and promotes heart morphogenesis in zebrafish development. *Cardiovasc. Res.* **cvab004**. doi:10.1093/cvr/cvab004

Desgrange, A., Le Garrec, J.-F. and Meilhac, S. M. (2018). Left-right asymmetry in heart development and disease: forming the right loop. *Development* **145**, dev162776. doi:10.1242/dev.162776

Dietrich, A.-C., Lombardo, V. A., Veerkamp, J., Priller, F. and Abdelilah-Seyfried, S. (2014). Blood flow and Bmp signaling control endocardial chamber morphogenesis. *Dev. Cell* **30**, 367-377. doi:10.1016/j.devcel.2014.06.020

Dobbs-McAuliffe, B., Zhao, Q. and Linney, E. (2004). Feedback mechanisms regulate retinoic acid production and degradation in the zebrafish embryo. *Mech. Dev.* **121**, 339-350. doi:10.1016/j.mod.2004.02.008

Dobrokhotov, O., Samsonov, M., Sokabe, M. and Hirata, H. (2018). Mechanoregulation and pathology of YAP/TAZ via Hippo and non-Hippo mechanisms. *Clin. Transl. Med.* **7**, e23. doi:10.1186/s40169-018-0202-9

Domogatskaya, A., Rodin, S. and Tryggvason, K. (2012). Functional diversity of laminins. *Annu. Rev. Cell Dev. Biol.* **28**, 523-553. doi:10.1146/annurev-cellbio-101011-155750

Dreos, R., Ambrosini, G., Périer, R. C. and Bucher, P. (2015). The Eukaryotic Promoter Database: expansion of EPDnew and new promoter analysis tools. *Nucleic Acids Res.* **43**, D92-D96. doi:10.1093/nar/gku1111

Dreos, R., Ambrosini, G., Groux, R., Cavin Périer, R. and Bucher, P. (2017). The eukaryotic promoter database in its 30th year: focus on non-vertebrate organisms. *Nucleic Acids Res.* **45**, D51-D55. doi:10.1093/nar/gkw1069.

- Duong, T. B., Holowiecki, A. and Waxman, J. S. (2021). Retinoic acid signaling restricts the size of the first heart field within the anterior lateral plate mesoderm. *Dev. Biol.* **473**, 119–129. doi:10.1016/j.ydbio.2021.02.005
- El-Brolosy, M. A., Kontarakis, Z., Rossi, A., Kuenne, C., Günther, S., Fukuda, N., Kikhi, K., Boezio, G. L. M., Takacs, C. M., Lai, S.-L. et al. (2019). Genetic compensation triggered by mutant mRNA degradation. *Nature* **568**, 193–197. doi:10.1038/s41586-019-1064-z
- Engler, A. J., Carag-Krieger, C., Johnson, C. P., Raab, M., Tang, H.-Y., Speicher, D. W., Sanger, J. W., Sanger, J. M. and Discher, D. E. (2008). Embryonic cardiomyocytes beat best on a matrix with heart-like elasticity: scar-like rigidity inhibits beating. *J. Cell Sci.* **121**, 3794–3802. doi:10.1242/jcs.029678
- Felker, A., Prummel, K. D., Merks, A. M., Mickoleit, M., Brombacher, E. C., Huisken, J., Panáková, D. and Mosimann, C. (2018). Continuous addition of progenitors forms the cardiac ventricle in zebrafish. *Nat. Commun.* **9**, 2001. doi:10.1038/s41467-018-04402-6
- Francou, A. and Kelly, R. (2016). Properties of cardiac progenitor cells in the second heart field. In *Etiology and Morphogenesis of Congenital Heart Disease: From Gene Function and Cellular Interaction to Morphology* (ed. T. Nakanishi, R. R. Markwald, H. S. Baldwin, B. B. Keller, D. Srivastava and H. Yamagishi), Chapter 23. Springer.
- Francou, A., Saint-Michel, E., Mesbah, K. and Kelly, R. G. (2014). TBX1 regulates epithelial polarity and dynamic basal filopodia in the second heart field. *Development* **141**, 4320–4331. doi:10.1242/dev.115022
- Francou, A., De Bono, C. and Kelly, R. G. (2017). Epithelial tension in the second heart field promotes mouse heart tube elongation. *Nat. Commun.* **8**, 14770. doi:10.1038/ncomms14770
- Fukui, H., Miyazaki, T., Chow, R. W.-Y., Ishikawa, H., Nakajima, H., Vermot, J. and Mochizuki, N. (2018). Hippo signaling determines the number of venous pole cells that originate from the anterior lateral plate mesoderm in zebrafish. *eLife* **7**, e29106. doi:10.7554/eLife.29106
- Fürthauer, M., Reifers, F., Brand, M., Thisse, B. and Thisse, C. (2001). sprouty4 acts in vivo as a feedback-induced antagonist of FGF signaling in zebrafish. *Development* **128**, 2175–2186. doi:10.1242/dev.128.12.2175
- Galloway, J. L., Wingert, R. A., Thisse, C., Thisse, B. and Zon, L. I. (2005). Loss of gata1 but not gata2 converts erythropoiesis to myelopoiesis in zebrafish embryos. *Dev. Cell* **8**, 109–116. doi:10.1016/j.devcel.2004.12.001
- Haag, T. A., Haag, N. P., Lekven, A. C. and Hartenstein, V. (1999). The role of cell adhesion molecules in *Drosophila* heart morphogenesis: faint sausage, Shotgun/DE-Cadherin, and Laminin AAre required for discrete stages in heart development. *Dev. Biol.* **208**, 56–69. doi:10.1006/dbio.1998.9188
- Hami, D., Grimes, A. C., Tsai, H.-J. and Kirby, M. L. (2011). Zebrafish cardiac development requires a conserved secondary heart field. *Development* **138**, 2389–2398. doi:10.1242/dev.061473
- Heckel, E., Boselli, F., Roth, S., Krudewig, A., Belting, H.-G., Charvin, G. and Vermot, J. (2015). Oscillatory flow modulates mechanosensitive klf2a expression through trpv4 and trpp2 during heart valve development. *Curr. Biol.* **25**, 1354–1361. doi:10.1016/j.cub.2015.03.038
- Hilenski, L. L., Terracio, L., Sawyer, R. and Borg, T. K. (1989). Effects of extracellular matrix on cytoskeletal and myofibrillar organization in vitro. *Scanning Microsc.* **3**, 535–548.
- Hochgreb-Hägele, T., Yin, C., Koo, D. E. S., Bronner, M. E. and Stainier, D. Y. R. (2013). Laminin β 1a controls distinct steps during the establishment of digestive organ laterality. *Development* **140**, 2734–2745. doi:10.1242/dev.097618
- Hruscha, A., Krawitz, P., Rechenberg, A., Heinrich, V., Hecht, J., Haass, C. and Schmid, B. (2013). Efficient CRISPR/Cas9 genome editing with low off-target effects in zebrafish. *Development* **140**, 4982–4987. doi:10.1242/dev.099085
- Hsu, J. J., Vedula, V., Baek, K. I., Chen, C., Chen, J., Chou, M. I., Lam, J., Subhedar, S., Wang, J., Ding, Y. et al. (2019). Contractile and hemodynamic forces coordinate Notch1b-mediated outflow tract valve formation. *JCI Insight* **4**, e124460. doi:10.1172/jci.insight.124460
- Huang, C.-J., Tu, C.-T., Hsiao, C.-D., Hsieh, F.-J. and Tsai, H.-J. (2003). Germ-line transmission of a myocardium-specific GFP transgene reveals critical regulatory elements in the cardiac myosin light chain 2 promoter of zebrafish. *Dev. Dyn.* **228**, 30–40. doi:10.1002/dvdy.10356
- Humphrey, J. D., Dufresne, E. R. and Schwartz, M. A. (2014). Mechanotransduction and extracellular matrix homeostasis. *Nat. Rev. Mol. Cell Biol.* **15**, 802–812. doi:10.1038/nrm3896
- Jacoby, A. S., Busch-Nentwich, E., Bryson-Richardson, R. J., Hall, T. E., Berger, J., Berger, S., Sonntag, C., Sachs, C., Geisler, R., Stemple, D. L. et al. (2009). The zebrafish dystrophic mutant softy maintains muscle fibre viability despite basement membrane rupture and muscle detachment. *Development* **136**, 3367–3376. doi:10.1242/dev.034561
- Kalogirou, S., Malissov, N., Moro, E., Argenton, F., Stainier, D. Y. R. and Beis, D. (2014). Intracardiac flow dynamics regulate atrioventricular valve morphogenesis. *Cardiovasc. Res.* **104**, 49–60. doi:10.1093/cvr/cvu186
- Kelly, R. G. (2012). The second heart field. *Curr. Top. Dev. Biol.* **100**, 33–65. doi:10.1016/B978-0-12-387786-4.00002-6
- Kelly, R. G., Brown, N. A. and Buckingham, M. E. (2001). The arterial pole of the mouse heart forms from Fgf10-expressing cells in pharyngeal mesoderm. *Dev. Cell* **1**, 435–440. doi:10.1016/S1534-5807(01)00040-5
- Kern, C. B., Norris, R. A., Thompson, R. P., Argraves, W. S., Fairey, S. E., Reyes, L., Hoffman, S., Markwald, R. R. and Mjaatvedt, C. H. (2007). Versican proteolysis mediates myocardial regression during outflow tract development. *Dev. Dyn.* **236**, 671–683. doi:10.1002/dvdy.21059
- Kettleborough, R. N. W., Busch-Nentwich, E. M., Harvey, S. A., Dooley, C. M., de Bruijn, E., van Eeden, F., Sealy, I., White, R. J., Herd, C., Nijman, I. J. et al. (2013). A systematic genome-wide analysis of zebrafish protein-coding gene function. *Nature* **496**, 494–497. doi:10.1038/nature11992
- Kimmel, C. B., Ballard, W. W., Kimmel, S. R., Ullmann, B. and Schilling, T. F. (1995). Stages of embryonic development of the zebrafish. *Dev. Dyn.* **203**, 253–310. doi:10.1002/aja.1002030302
- Knight, H. G. and Yelon, D. (2016). Utilizing zebrafish to understand second heart field development. In *Etiology and Morphogenesis of Congenital Heart Disease: From Gene Function and Cellular Interaction to Morphology* (ed. T. Nakanishi, R. R. Markwald, H. S. Baldwin, B. B. Keller, D. Srivastava and H. Yamagishi), Chapter 25. Springer.
- Knöll, R., Postel, R., Wang, J., Krätzner, R., Hennecke, G., Vacaru, A. M., Vakeel, P., Schubert, C., Murthy, K., Rana, B. K. et al. (2007). Laminin- α 4 and integrin-linked kinase mutations cause human cardiomyopathy via simultaneous defects in cardiomyocytes and endothelial cells. *Circulation* **116**, 515–525. doi:10.1161/CIRCULATIONAHA.107.689984
- Labun, K., Montague, T. G., Gagnon, J. A., Thyme, S. B. and Valen, E. (2016). CHOPCHOP v2: a web tool for the next generation of CRISPR genome engineering. *Nucleic Acids Res.* **44**, W272–W276. doi:10.1093/nar/gkw398
- Langheinrich, U., Hennen, E., Stott, G. and Vacun, G. (2002). Zebrafish as a model organism for the identification and characterization of drugs and genes affecting p53 signaling. *Curr. Biol.* **12**, 2023–2028. doi:10.1016/S0960-9822(02)01319-2
- Lazic, S. and Scott, I. C. (2011). Mef2cb regulates late myocardial cell addition from a second heart field-like population of progenitors in zebrafish. *Dev. Biol.* **354**, 123–133. doi:10.1016/j.ydbio.2011.03.028
- Li, D., Sinha, T., Ajima, R., Seo, H.-S., Yamaguchi, T. P. and Wang, J. (2016). Spatial regulation of cell cohesion by Wnt5a during second heart field progenitor deployment. *Dev. Biol.* **412**, 18–31. doi:10.1016/j.ydbio.2016.02.017
- Mably, J. D., Chuang, L. P., Serluca, F. C., Mohideen, M.-A. P. K., Chen, J.-N. and Fishman, M. C. (2006). santa and valentine pattern concentric growth of cardiac myocardium in the zebrafish. *Development* **133**, 3139–3146. doi:10.1242/dev.02469
- Miner, J. H., Li, C., Mudd, J. L., Go, G. and Sutherland, A. E. (2004). Compositional and structural requirements for laminin and basement membranes during mouse embryo implantation and gastrulation. *Development* **131**, 2247–2256. doi:10.1242/dev.01112
- Mittal, A., Pulina, M., Hou, S.-Y. and Astrof, S. (2010). Fibronectin and integrin alpha 5 play essential roles in the development of the cardiac neural crest. *Mech. Dev.* **127**, 472–484. doi:10.1016/j.mod.2010.08.005
- Mittal, A., Pulina, M., Hou, S.-Y. and Astrof, S. (2013). Fibronectin and integrin alpha 5 play requisite roles in cardiac morphogenesis. *Dev. Biol.* **381**, 73–82. doi:10.1016/j.ydbio.2013.06.010
- Mittal, N., Yoon, S. H., Enomoto, H., Hiroshi, M., Shimizu, A., Kawakami, A., Fujita, M., Watanabe, H., Fukuda, K. and Makino, S. (2019). Versican is crucial for the initiation of cardiovascular lumen development in medaka (*Oryzias latipes*). *Sci. Rep.* **9**, 9475. doi:10.1038/s41598-019-45851-3
- Mjaatvedt, C. H., Yamamura, H., Capehart, A. A., Turner, D. and Markwald, R. R. (1998). The Cspg2 gene, disrupted in the hfd mutant, is required for right cardiac chamber and endocardial cushion formation. *Dev. Biol.* **202**, 56–66. doi:10.1006/dbio.1998.9001
- Mjaatvedt, C. H., Nakaoka, T., Moreno-Rodriguez, R., Norris, R. A., Kern, M. J., Eisenberg, C. A., Turner, D. and Markwald, R. R. (2001). The outflow tract of the heart is recruited from a novel heart-forming field. *Dev. Biol.* **238**, 97–109. doi:10.1006/dbio.2001.0409
- Montague, T. G., Cruz, J. M., Gagnon, J. A., Church, G. M. and Valen, E. (2014). CHOPCHOP: a CRISPR/Cas9 and TALEN web tool for genome editing. *Nucleic Acids Res.* **42**, W401–W407. doi:10.1093/nar/gku410
- Morton, S. U., Scherz, P. J., Cordes, K. R., Ivey, K. N., Stainier, D. Y. R. and Srivastava, D. (2008). microRNA-138 modulates cardiac patterning during embryonic development. *Proc. Natl. Acad. Sci. USA* **105**, 17830–17835. doi:10.1073/pnas.0804673105
- Mouw, J. K., Ou, G. and Weaver, V. M. (2014). Extracellular matrix assembly: a multiscale deconstruction. *Nat. Rev. Mol. Cell Biol.* **15**, 771–785. doi:10.1038/nrm3902
- Niederreither, K., McCaffery, P., Dräger, U. C., Chambon, P. and Dollé, P. (1997). Restricted expression and retinoic acid-induced downregulation of the retinaldehyde dehydrogenase type 2 (RALDH-2) gene during mouse development. *Mech. Dev.* **62**, 67–78. doi:10.1016/S0925-4773(96)00653-3
- Niederreither, K., Vermot, J., Messaddeq, N., Schuhbauer, B., Chambon, P. and Dollé, P. (2001). Embryonic retinoic acid synthesis is essential for heart morphogenesis in the mouse. *Development* **128**, 1019–1031. doi:10.1242/dev.128.7.1019
- Noël, E. S., Verhoeven, M., Lagendijk, A. K., Tessadori, F., Smith, K., Choorapoikayil, S., den Hertog, J. and Bakkers, J. (2013). A Nodal-

- independent and tissue-intrinsic mechanism controls heart-looping chirality. *Nat. Commun.* **4**, 2754. doi:10.1038/ncomms3754
- Novodvorsky, P., Watson, O., Gray, C., Wilkinson, R. N., Reeve, S., Smythe, C., Beniston, R., Plant, K., Maguire, R. M. K., Rothman, A. et al.** (2015). *klf2ash317* mutant zebrafish do not recapitulate morpholino-induced vascular and haematopoietic phenotypes. *PLoS ONE* **10**, e0141611. doi:10.1371/journal.pone.0141611
- Odenthal, J., Haffter, P., Vogelsang, E., Brand, M., van Eeden, F. J., Furutani-Seiki, M., Granato, M., Hammerschmidt, M., Heisenberg, C. P., Jiang, Y. J. et al.** (1996). Mutations affecting the formation of the notochord in the zebrafish, *Danio rerio*. *Development* **123**, 103-115. doi:10.1242/dev.123.1.103
- Parsons, M. J., Pollard, S. M., Saúde, L., Feldman, B., Coutinho, P., Hirst, E. M. A. and Stemple, D. L.** (2002). Zebrafish mutants identify an essential role for laminins in notochord formation. *Development* **129**, 3137-3146. doi:10.1242/dev.129.13.3137
- Quinkertz, A. and Campos-Ortega, J. A.** (1999). A new β -globin gene from the zebrafish, βE_1 , and its pattern of transcription during embryogenesis. *Dev. Genes Evol.* **209**, 126-131. doi:10.1007/s004270050235
- Reischauer, S., Arnaout, R., Ramadass, R. and Stainier, D. Y. R.** (2014). Actin binding GFP allows 4D in vivo imaging of myofilament dynamics in the zebrafish heart and the identification of *ErbB2* signaling as a remodeling factor of myofibril architecture. *Circ. Res.* **115**, 845-856. doi:10.1161/CIRCRESAHA.115.304356
- Rochais, F., Mesbah, K. and Kelly, R. G.** (2009). Signaling pathways controlling second heart field development. *Circ. Res.* **104**, 933-942. doi:10.1161/CIRCRESAHA.109.194464
- Roediger, M., Miosge, N. and Gersdorff, N.** (2010). Tissue distribution of the laminin $\beta 1$ and $\beta 2$ chain during embryonic and fetal human development. *J. Mol. Histol.* **41**, 177-184. doi:10.1007/s10735-010-9275-5
- Rottbauer, W., Saurin, A. J., Lickert, H., Shen, X., Burns, C. G., Wo, Z. G., Kemler, R., Kingstone, R., Wu, C. and Fishman, M.** (2002). Reptin and pontin antagonistically regulate heart growth in zebrafish embryos. *Cell* **111**, 661-672. doi:10.1016/S0092-8674(02)01112-1
- Ryckebusch, L., Wang, Z., Bertrand, N., Lin, S.-C., Chi, X., Schwartz, R., Zaffran, S. and Niederreither, K.** (2008). Retinoic acid deficiency alters second heart field formation. *Proc. Natl Acad. Sci. USA* **105**, 2913-2918. doi:10.1073/pnas.0712344105
- Rydeen, A. B. and Waxman, J. S.** (2016). Cyp26 enzymes facilitate second heart field progenitor addition and maintenance of ventricular integrity. *PLoS Biol.* **14**, e2000504. doi:10.1371/journal.pbio.2000504
- Sampaolo, S., Napolitano, F., Tirozzi, A., Reccia, M. G., Lombardi, L., Farina, O., Barra, A., Cirillo, F., Melone, M. A. B., Gianfrancesco, F. et al.** (2017). Identification of the first dominant mutation of LAMA5 gene causing a complex multisystem syndrome due to dysfunction of the extracellular matrix. *J. Med. Genet.* **54**, 710. doi:10.1136/jmedgenet-2017-104555
- Samsa, L. A., Givens, C., Tzima, E., Stainier, D. Y. R., Qian, L. and Liu, J.** (2015). Cardiac contraction activates endocardial Notch signaling to modulate chamber maturation in zebrafish. *Development* **142**, 4080-4091. doi:10.1242/dev.125724
- Schéele, S., Nyström, A., Durbeek, M., Talts, J. F., Ekblom, M. and Ekblom, P.** (2007). Laminin isoforms in development and disease. *J. Mol. Med.* **85**, 825-836. doi:10.1007/s00109-007-0182-5
- Sehnert, A. J., Huq, A., Weinstein, B. M., Walker, C., Fishman, M. and Stainier, D. Y. R.** (2002). Cardiac troponin T is essential in sarcomere assembly and cardiac contractility. *Nat. Genet.* **31**, 106-110. doi:10.1038/ng875
- Sirbu, I. O., Zhao, X. and Duester, G.** (2008). Retinoic acid controls heart anteroposterior patterning by down-regulating *Isl1* through the *Fgf8* pathway. *Dev. Dyn.* **237**, 1627-1635. doi:10.1002/dvdy.21570
- Smyth, N., Vatanserver, H. S., Murray, P., Meyer, M., Frie, C., Paulsson, M. and Edgar, D.** (1999). Absence of basement membranes after targeting the LAMC1 gene results in embryonic lethality due to failure of endoderm differentiation. *J. Cell Biol.* **144**, 151-160. doi:10.1083/jcb.144.1.151
- Staudt, D. W., Liu, J., Thorn, K. S., Stuurman, N., Liebling, M. and Stainier, D. Y. R.** (2014). High-resolution imaging of cardiomyocyte behavior reveals two distinct steps in ventricular trabeculation. *Development* **141**, 585-593. doi:10.1242/dev.098632
- Steed, E., Faggianelli, N., Roth, S., Ramspacher, C., Concordet, J.-P. and Vermot, J.** (2016). *klf2a* couples mechanotransduction and zebrafish valve morphogenesis through fibronectin synthesis. *Nat. Commun.* **7**, 11646. doi:10.1038/ncomms11646
- Sztaf, T., Berger, S., Currie, P. D. and Hall, T. E.** (2011). Characterization of the laminin gene family and evolution in zebrafish. *Dev. Dyn.* **240**, 422-431. doi:10.1002/dvdy.22537
- Thybol, J., Kortessmaa, J., Cao, R., Soininen, R., Wang, L., Iivanainen, A., Sorokin, L., Risling, M., Cao, Y. and Tryggvason, K.** (2002). Deletion of the laminin $\alpha 4$ chain leads to impaired microvessel maturation. *Mol. Cell. Biol.* **22**, 1194-1202. doi:10.1128/MCB.22.4.1194-1202.2002
- Triedman, J. K. and Newburger, J. W.** (2016). Trends in congenital heart disease. *Circulation* **133**, 2716-2733. doi:10.1161/CIRCULATIONAHA.116.023544
- Vanwinkle, W. B., Snuggs, M. B. and Bujas, L. M.** (1996). Cardiogel: a biosynthetic extracellular matrix for cardiomyocyte culture. *In Vitro Cell. Dev. Biol. Anim.* **32**, 478-485. doi:10.1007/BF02723051
- Vermot, J., Forouhar, A. S., Liebling, M., Wu, D., Plummer, D., Gharib, M. and Fraser, S. E.** (2009). Reversing blood flows act through *klf2a* to ensure normal valvulogenesis in the developing heart. *PLoS Biol.* **7**, e1000246. doi:10.1371/journal.pbio.1000246
- Vikhorev, P. G. and Vikhoreva, N. N.** (2018). Cardiomyopathies and related changes in contractility of human heart muscle. *Int. J. Mol. Sci.* **19**, 2234. doi:10.3390/ijms19082234
- Waldo, K. L., Kumiski, D. H., Wallis, K. T., Stadt, H. A., Hutson, M. R., Platt, D. H. and Kirby, M. L.** (2001). Conotruncal myocardium arises from a secondary heart field. *Development* **128**, 3179-3188. doi:10.1242/dev.128.16.3179
- Wang, J., Hoshijima, M., Lam, J., Zhou, Z., Jokieli, A., Dalton, N. D., Hultenby, K., Ruiz-Lozano, P., Ross, J., Jr, Tryggvason, K. et al.** (2006). Cardiomyopathy associated with microcirculation dysfunction in laminin $\alpha 4$ chain-deficient mice. *J. Biol. Chem.* **281**, 213-220. doi:10.1074/jbc.M505061200
- Waxman, J. S., Keegan, B. R., Roberts, R. W., Poss, K. D. and Yelon, D.** (2008). *Hoxb5b* acts downstream of retinoic acid signaling in the forelimb field to restrict heart field potential in zebrafish. *Dev. Cell* **15**, 923-934. doi:10.1016/j.devcel.2008.09.009
- Welten, M. C. M., de Haan, S. B., van den Boogert, N., Noordermeer, J. N., Lamers, G. E. M., Spaik, H. P., Meijer, A. H. and Verbeek, F. J.** (2006). ZebraFISH: fluorescent in situ hybridization protocol and three-dimensional imaging of gene expression patterns. *Zebrafish* **3**, 465-476. doi:10.1089/zeb.2006.3.465
- Wu, R. S., Lam, I. I., Clay, H., Duong, D. N., Deo, R. C. and Coughlin, S. R.** (2018). A rapid method for directed gene knockout for screening in G0 zebrafish. *Dev. Cell* **46**, 112-125.e4. doi:10.1016/j.devcel.2018.06.003
- Yamamura, H., Zhang, M., Markwald, R. R. and Mjaatvedt, C. H.** (1997). A heart segmental defect in the anterior-posterior axis of a transgenic mutant mouse. *Dev. Biol.* **186**, 58-72. doi:10.1006/dbio.1997.8559
- Yarnitzky, T. and Volk, T.** (1995). Laminin is required for heart, somatic muscles, and gut development in the *Drosophila* embryo. *Dev. Biol.* **169**, 609-618. doi:10.1006/dbio.1995.1173
- Yelon, D., Horne, S. A. and Stainier, D. Y. R.** (1999). Restricted expression of cardiac myosin genes reveals regulated aspects of heart tube assembly in zebrafish. *Dev. Biol.* **214**, 23-37. doi:10.1006/dbio.1999.9406
- Yurchenco, P. D., Quan, Y., Colognato, H., Mathus, T., Harrison, D., Yamada, Y. and O'Rear, J. J.** (1997). The α chain of laminin-1 is independently secreted and drives secretion of its β - and γ -chain partners. *Proc. Natl. Acad. Sci. USA* **94**, 10189-10194. doi:10.1073/pnas.94.19.10189
- Zaffran, S., Robrini, N. E. and Bertrand, N.** (2014). Retinoids and cardiac development. *J. Dev. Biol.* **2**, 50-71. doi:10.3390/jdb2010050
- Zhang, R., Cao, P., Yang, Z., Wang, Z., Wu, J.-L., Chen, Y. and Pan, Y.** (2015). Heparan sulfate biosynthesis enzyme, *Ext1*, contributes to outflow tract development of mouse heart via modulation of FGF signaling. *PLoS ONE* **10**, e0136518. doi:10.1371/journal.pone.0136518
- Zhou, Y., Cashman, T. J., Nevis, K. R., Obregon, P., Carney, S. A., Liu, Y., Gu, A., Mosimann, C., Sondalle, S., Peterson, R. E. et al.** (2011). Latent TGF- β binding protein 3 identifies a second heart field in zebrafish. *Nature* **474**, 645-648. doi:10.1038/nature10094

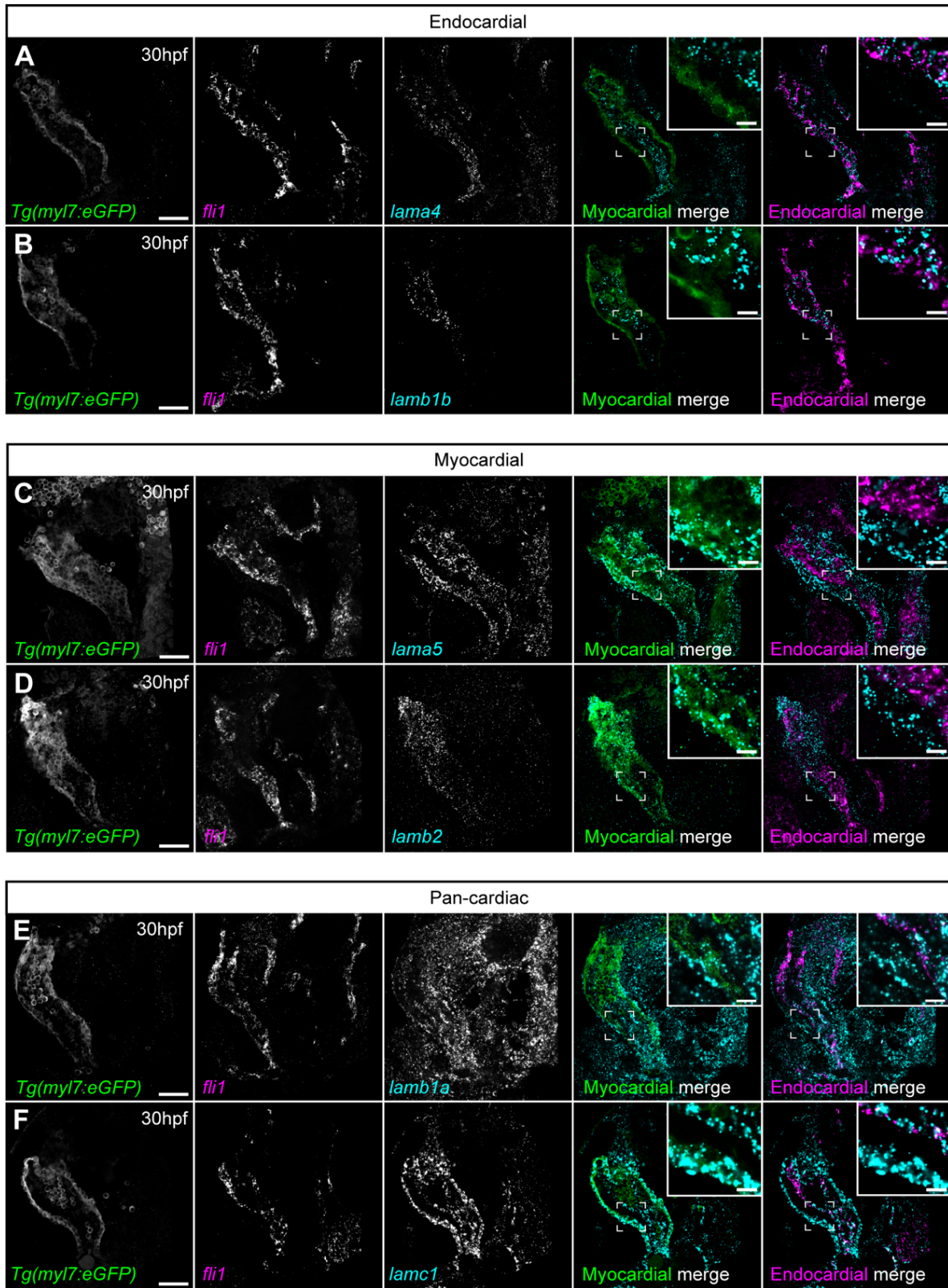


Fig. S1. Laminin subunits exhibit tissue-specific expression

A-F: Single z-plane confocal images of fluorescent mRNA *in situ* hybridization analysis of *lama4*, *lamb1b*, *lama5*, *lamb2*, *lamb1a* or *lamc1* expression (cyan) in *Tg(myl7:eGFP)* embryos (myocardium, green) counterstained for *fli1* mRNA (endocardium, magenta). *lama4* and *lamb1b* expression colocalises with *fli1* in the endocardium (A,B), while *lama5* and *lamb2* are expressed in the myocardium (C,D). *lamb1a* and *lamc1* are expressed in both myocardial and endocardial cells (E,F). Scale bars main panels: 50µm, insets: 10µm.

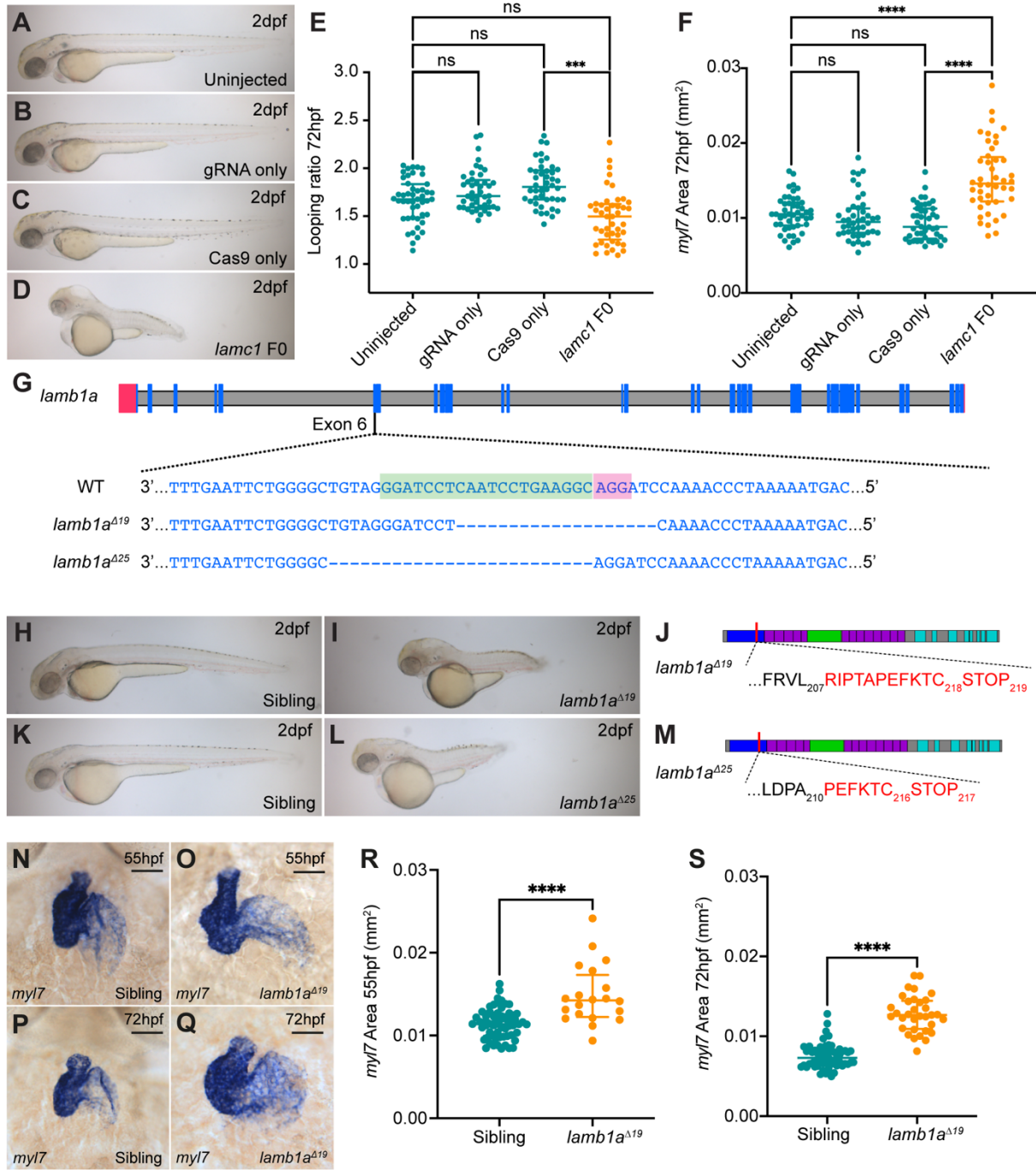


Fig. S2. *lamc1* and *lambla* mutants have defects in heart morphogenesis

A-D: Brightfield images of uninjected control (A), gRNA- or Cas9-only injected controls (B,C) or *lamc1* F0 crispant embryos (D) at 2dpf. Lateral views, anterior to left. E-F: Quantification of looping ratio (E) and heart size (F) in uninjected embryos (n=47), gRNA only control embryos (n=44), Cas9 only control embryos (n=44), and *lamc1* crispants (n=44) at 72hpf. Kruskal-Wallis test. G: Schematic depicting *lambla* gene (danRer10/GRCz10), with non-coding exons in red and coding exons in blue. gRNA target site (green) is located in exon 6 of wild type (WT) *lambla* (magenta indicates PAM sequence), and 2 deletion alleles of 19bp and 25bp were recovered. H-L: Brightfield images of sibling embryos (H,K), *lambla*^{A19} (I) and *lambla*^{A25} mutant embryos (L) and 2dpf. J,M: Schematic representation of Lamb1a protein structure (UniProt Q8JHV7), with the alterations in amino acid sequence depicted in red. Both *lambla* mutant alleles result in frameshift and insertion of a stop codon. N-Q: mRNA *in situ* hybridization analysis of *myl7* expression in sibling (N,P) and *lambla*^{A19} mutant embryos (O,Q) and 55hpf and 72hpf. Ventral views, anterior to top. R-S: Quantification of *myl7* area reveals a significant increase in heart size in *lambla* mutants (55hpf: n=20; 72hpf: n=33) when compared to siblings (55hpf: n=62; 72hpf: n=62) at 55hpf and 72hpf. Median +/- interquartile range. Mann-Whitney test. **** = p < 0.0001, *** = p < 0.001, ** = p < 0.01. Scale bars: 50µm.

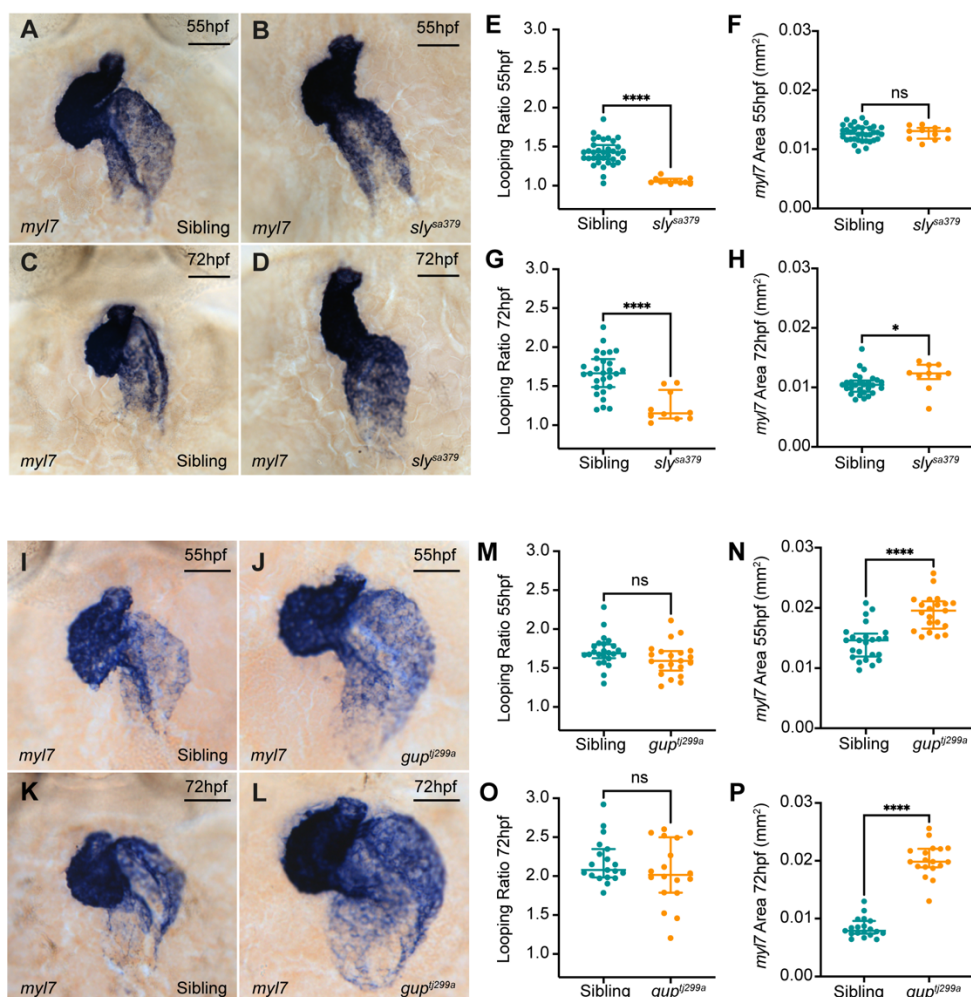


Fig. S3. *sleepy* and *grumpy* mutants recapitulate *lamc1* crispant and *lambla* mutant heart phenotypes

A-D: mRNA *in situ* hybridization analysis of *myl7* expression in sibling (A: n=35; C: n=28) and *sly^{sa379}* mutant embryos (B: n=11; D: n=10) at 55hpf and 72hpf. Ventral views, anterior to top. E-H: Quantification of looping ratio in sibling and *sly^{sa379}* mutant embryos reveals a reduction in heart looping morphology at both 55hpf (E) and 72hpf (G). Heart size is unaffected in *sly^{sa379}* mutant embryos compared to siblings at 55hpf (F), however *sly^{sa379}* mutants have slightly enlarged hearts at 72hpf (H). I-L: mRNA *in situ* hybridization analysis of *myl7* expression in sibling (I: n=24; K: n=19) and *gup^{tj299a}* mutant embryos (J: n=21; L: n=18) at 55hpf and 72hpf. Ventral views, anterior to top. M-P: Quantification of looping ratio reveals no significant difference in looping morphology between sibling and *gup^{tj299a}* mutant embryos (M,O). However, *gup^{tj299a}* mutant embryos exhibit enlarged hearts when compared to siblings at both 55hpf (N), and 72hpf (P). Median +/- interquartile range. Mann-Whitney test, **** = $p < 0.0001$, *** = $p < 0.001$, ** = $p < 0.01$, * = $p < 0.05$, ns = not significant. Scale bars: 50 μm.

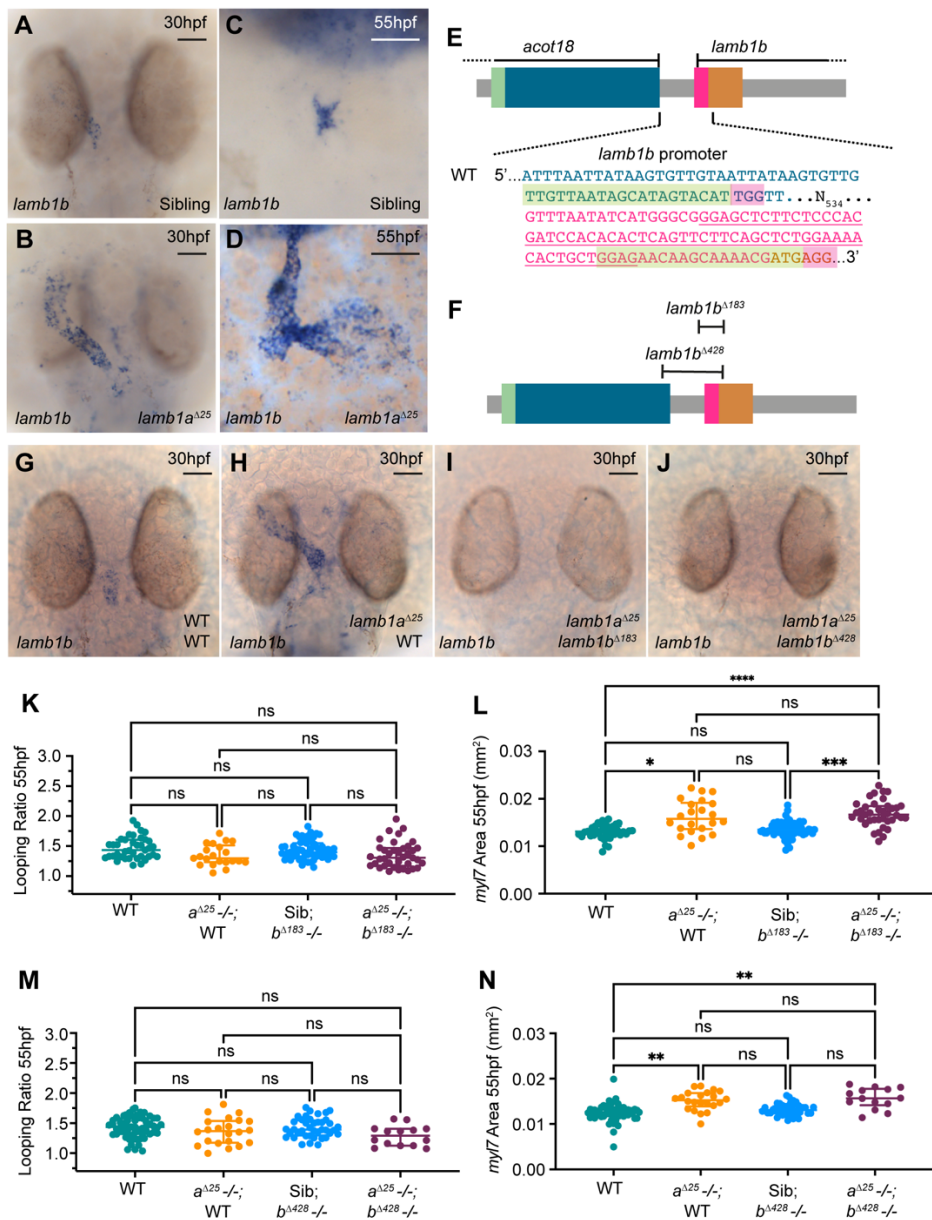


Fig. S4. *lamb1b* is dispensable for heart development

A-D: mRNA *in situ* hybridization expression analysis of *lamb1b* in sibling (A,C) and *lamb1a*^{A25} mutant embryos (B,D) at 30hpf and 55hpf. *lamb1a*^{A25} mutants exhibit an upregulation of *lamb1b* throughout the endocardium (30hpf: n=15/16; 55hpf: n=13/14) compared to wild types (30hpf: n=15/17; 55hpf: n=12/13) at both stages. A-B: Dorsal views, anterior to top; C-D: Ventral views, anterior to top. E-F: Schematic representation of CRISPR gRNAs (green sequence, PAM in magenta) targeting the promoter of *lamb1b* (danRer10/GRCz10). Two *lamb1b* deletion alleles were recovered: *lamb1b*^{A183} and *lamb1b*^{A428}. G-J: mRNA *in situ* hybridization analysis of *lamb1b* expression in wild type (G), *lamb1a*^{A25} mutants (H), *lamb1b*^{A183};*lamb1a*^{A25} double mutants (I), or *lamb1b*^{A428};*lamb1a*^{A25} double mutants (J). *lamb1b* expression is abrogated in both *lamb1b*^{A183};*lamb1a*^{A25} (n=6/6) and *lamb1b*^{A428};*lamb1a*^{A25} double mutants (n=6/6) (I,J). Dorsal views, anterior to top. K-L: Quantification of heart looping ratio (K) and *myl7* expression domain as a proxy for heart size (L) in wild type (n=39), *lamb1a*^{A25} single mutants (n=22), *lamb1b*^{A183} single mutants (n=62), and *lamb1b*^{A183};*lamb1a*^{A25} double mutant embryos (n=39) at 55hpf. M,N: Quantification of heart looping ratio (M) and heart size (N) in wild type (n=60), *lamb1a*^{A25} single mutants (n=22), *lamb1b*^{A428} single mutants (n=40), and *lamb1b*^{A428};*lamb1a*^{A25} double mutant embryos (n=14) at 55hpf. Loss of *lamb1b* in *lamb1a*^{A25} neither induces defects in heart looping morphology, nor rescues heart size, in *lamb1a*^{A25} mutants. Median +/- interquartile range. Kruskal Wallis test, * = p < 0.05, ns = not significant. Scale bars: 50µm.

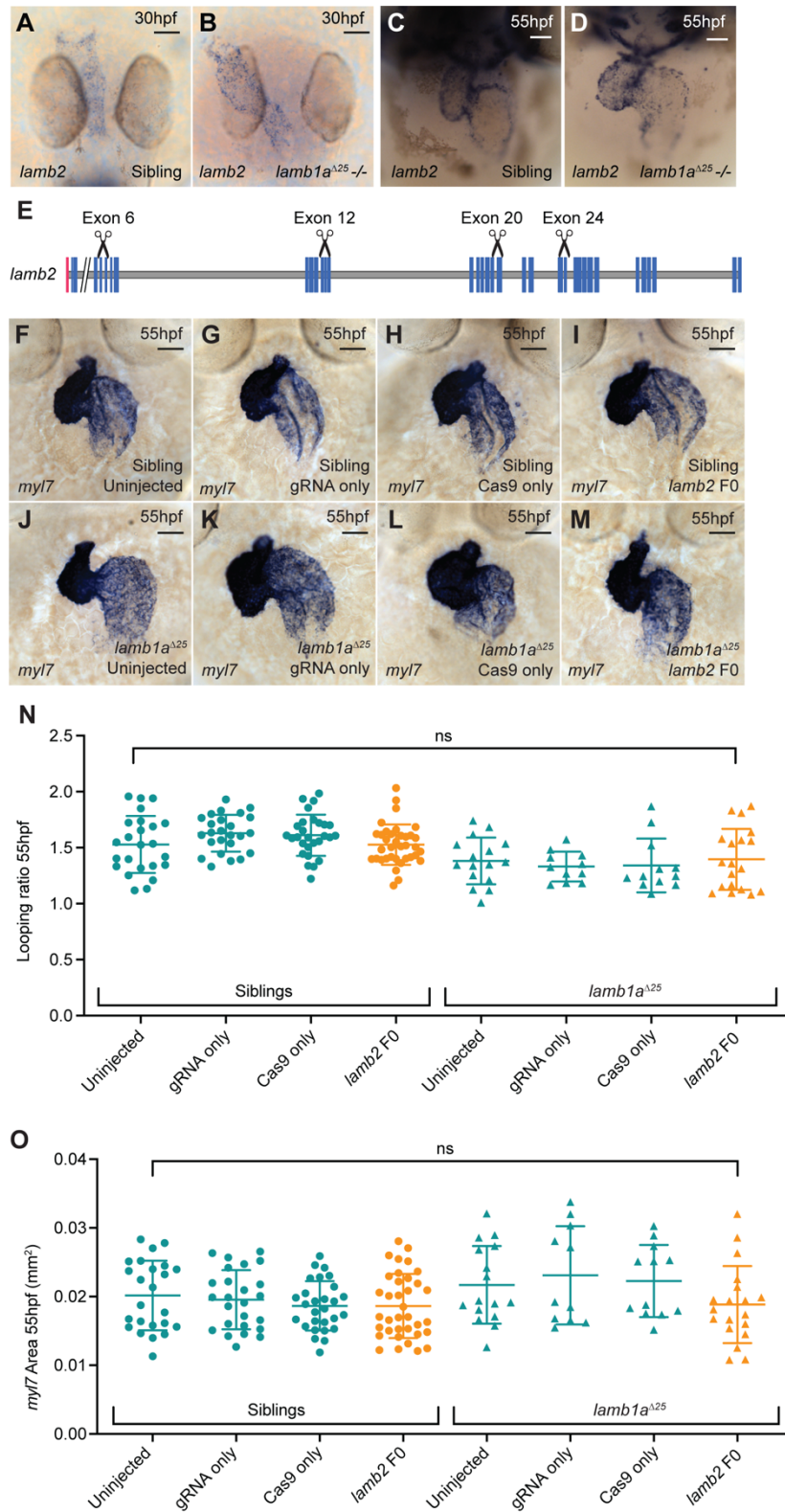


Fig. S5. *lamb2* does not compensate for loss of *lamb1a* in the developing heart A-D: mRNA *in situ* hybridization expression analysis of *lamb2* expression in the heart of sibling (A,C) and *lamb1a*^{A25} mutants (B,D) at 30hpf and 55hpf. At both 30hpf and 55hpf *lamb2* expression in *lamb1a*^{A25} mutants (B: 30hpf, n= 16/20; D: 55hpf, n=13/15) is comparable when compared to siblings (A: 30hpf, n=10/13; C: 55hpf, n=15/15). E: Schematic depicting *lamb2* gene (danRer10/GRCz10), with non-coding exons in red and coding exons in blue. 4 CRISPR gRNA target sites (scissors) were selected throughout the gene. F-M: mRNA *in situ* hybridization analysis of *myl7* expression at 55hpf in sibling and *lamb1a*^{A25} mutant embryos, either uninjected controls (F,J), controls injected with *lamb2*-targeting gRNAs only (G,K), controls injected with Cas9 protein only (H,L), or experimental samples with *lamb2*-targeting gRNAs together with Cas9 protein (*lamb2* F0, I,M). N-O: Quantitative analysis of looping ratio (N) and *myl7* area (O) at 55hpf in uninjected controls (siblings n=24, *lamb1a*^{A25} mutants n=16), gRNA-injected controls (siblings n=25, *lamb1a*^{A25} mutants n=11), Cas9-injected controls (siblings n=28, *lamb1a*^{A25} mutants n=12) and *lamb2* F0 crispants (siblings n=36, *lamb1a*^{A25} mutants n=19). No significant differences are observed between any experimental groups, indicating CRISPR-mediated mutagenesis of *lamb2* does not alter the *lamb1a* mutant phenotype. Median +/- interquartile range, Kruskal-Wallis test, ns = not significant.

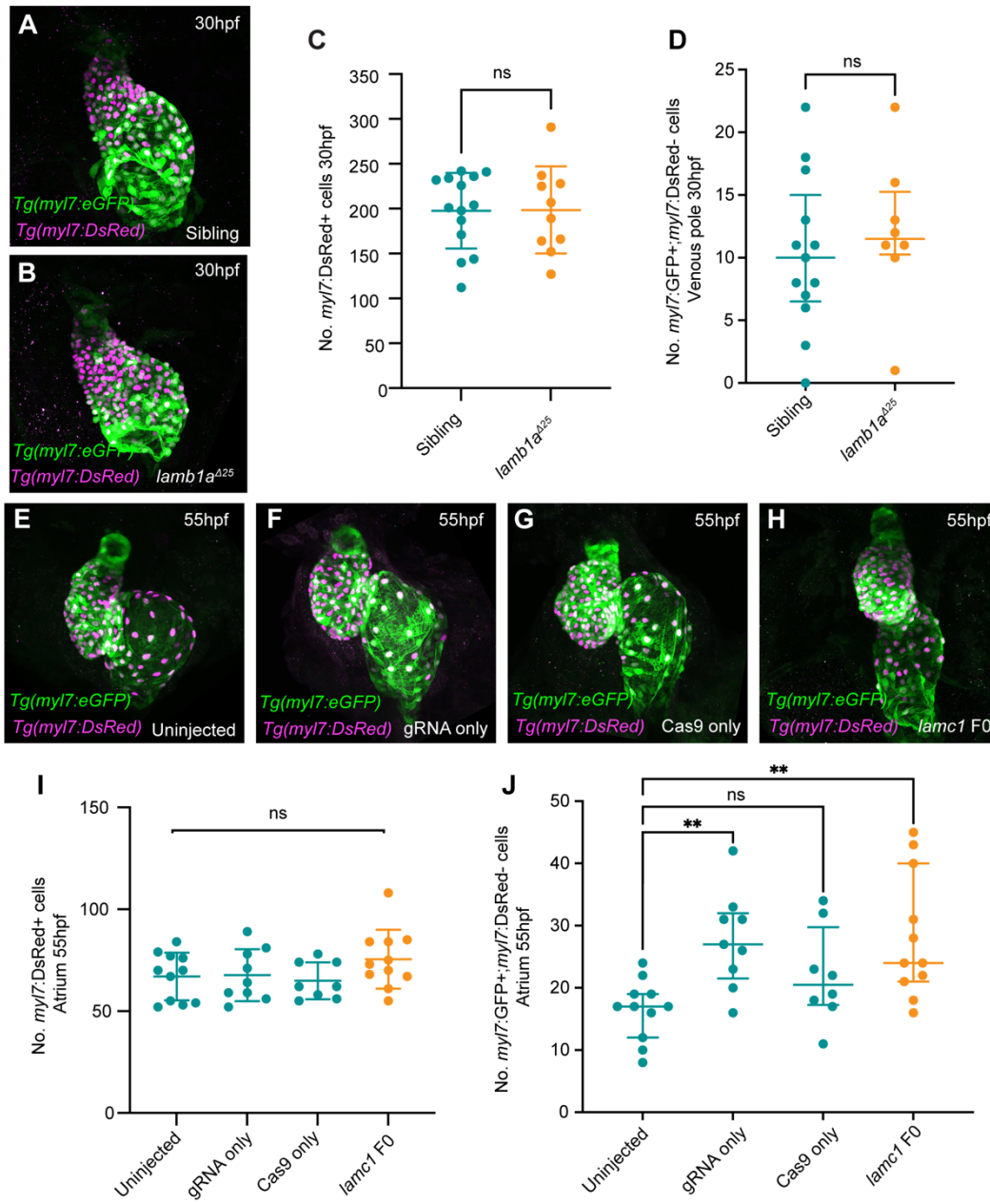


Fig. S6. Laminin restricts SHF addition during looping morphogenesis

A-B: Maximum intensity projections of confocal image z-stacks in *Tg(myl7:eGFP);Tg(myl7:DsRed)* double transgenic sibling (A) and *lambl α ^{A25}* mutant embryos (B) at 30hpf. C: Quantification of GFP+ DsRed+ cell number in the heart tube of sibling (n=14) and *lambl α ^{A25}* mutant embryos (n=10) at 30hpf reveals no significant difference in the number of dsRed+ cardiomyocytes. D: Quantification of GFP+;DsRed- SHF cell number in siblings (n=13) and *lambl α ^{A25}* mutants (n=8) at 30hpf reveals no change in newly-added SHF cells in *lambl α ^{A25}* mutants compared to siblings. E-H: Maximum intensity projections of confocal image z-stacks in *Tg(myl7:eGFP);Tg(myl7:DsRed)* double transgenic uninjected control (E), gRNA only injected controls (F), Cas9 only controls (G), and *lamc1* crispants (H) at 55hpf. I: Quantification of GFP+;DsRed+ cell number in the atrium of uninjected controls (n=11), gRNA only injected controls (n=9), Cas9 only injected controls (n=8) and *lamc1* F0 crispant embryos (n=11) at 55hpf. No significant differences in DsRed+ cell number in *lamc1* F0 crispants were observed. J: Quantification of GFP+;DsRed- SHF cell number at the venous pole in uninjected controls (n=11), gRNA only injected controls (n=9), Cas9 only injected controls (n=8) and *lamc1* F0 crispant embryos (n=11) at 55hpf reveals a significant increase in newly-added SHF cells to the venous pole in *lamc1* crispants when compared to uninjected controls. Horizontal bars indicate mean \pm s.d, C,D: Mann-Whitney test. I: Kruskal Wallis test. J: Brown-Forsythe and Welch ANOVA test, ** = $p < 0.01$, ns = not significant. Scale bars: 50 μ m.

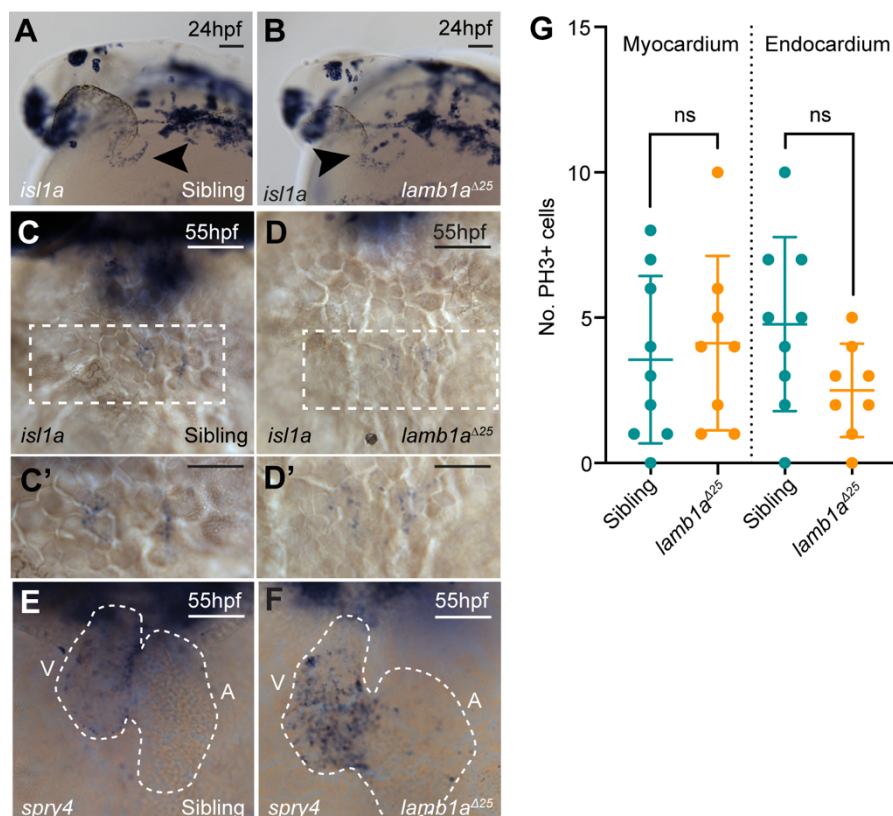


Fig. S7. *isll1* expression is unaffected and *spry4* is upregulated in *lamb1a* mutant embryos

A-D: mRNA *in situ* hybridization analysis of *isll1* expression at 24hpf (A,B) and 55hpf (C,D) in sibling and *lamb1a^{A25}* mutant embryos. The domain of *isll1* expression at the venous pole of the heart (black arrowhead) is unaffected in *lamb1a^{A25}* mutants (B, n=22/28; D, n=17/23) when compared to sibling embryos (A, n=23/29; C, n=38/47) at both stages. C',D': Higher magnification of venous pole region contained in white box in C and D. E-F: mRNA *in situ* hybridization analysis of *spry4* expression at 55hpf reveals a mild upregulation of *spry4* expression in *lamb1a^{A25}* mutants (F, n=10/21) when compared to siblings (E, n=48). G: Quantification of PH3-positive proliferation cells in the myocardium and endocardium of sibling (n=9) and *lamb1a^{A25}* mutant embryos (n=8) at 55hpf. There is no significant difference in proliferation upon loss of *lamb1a*. Mean \pm s.d., unpaired t test. Scale bars: 50 μ m.

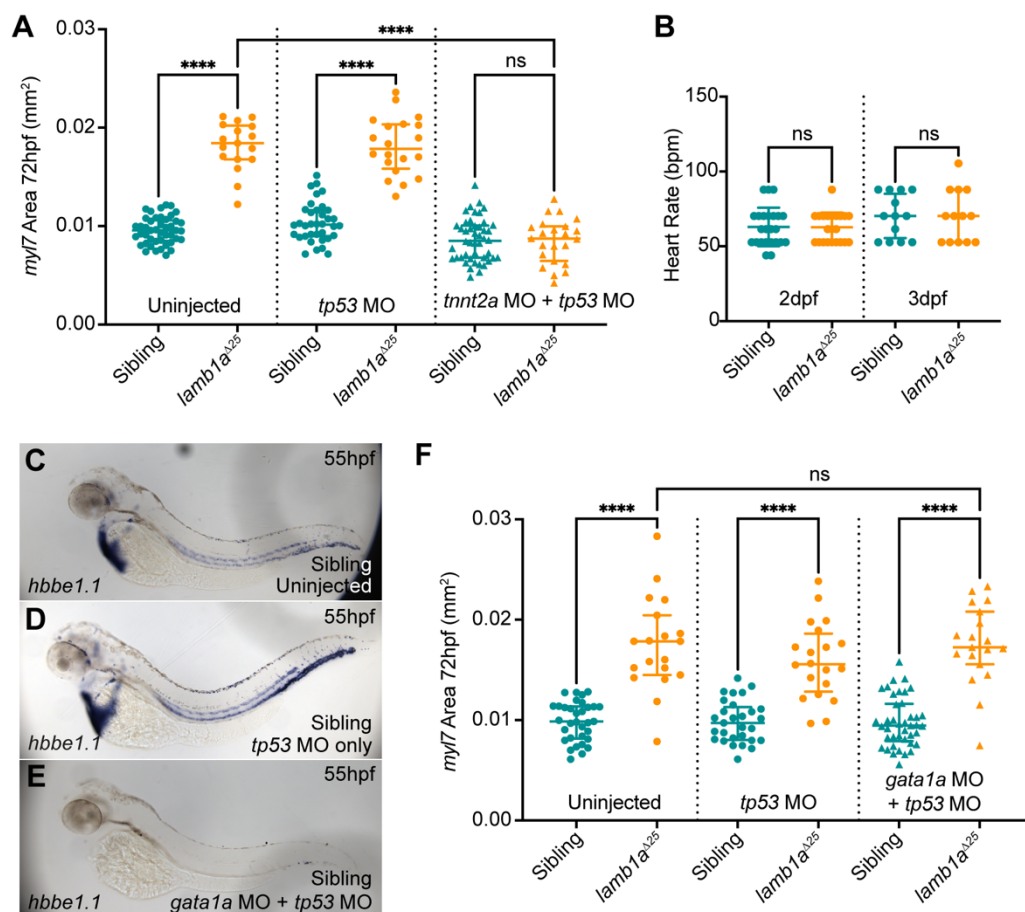


Fig. S8. Lamb1a restricts cardiac growth independent of haemodynamic force A: Quantification of *myl7* expression domain at 72hpf as a proxy for heart size in sibling and *lamb1a*^{Δ25} mutants, either uninjected (sibling: n=45; *lamb1a*^{Δ25} mutants: n=17), injected with *tp53* MO (sibling: n=36; *lamb1a*^{Δ25} mutant: n=20) or co-injected with *tp53* MO and *tnnt2a* MO (sibling: n=46; *lamb1a*^{Δ25} mutant: n=23). Cardiomegaly is rescued in *lamb1a*^{Δ25} mutants injected with *tnnt2a* MO. B: Quantification of heart rate in sibling and *lamb1a*^{Δ25} mutant embryos at 2dpf and 3dpf reveals that *lamb1a*^{Δ25} mutants do not exhibit an elevated heart rate. C-D: mRNA *in situ* hybridization analysis of *hbbe1.1* expression at 55hpf in sibling embryos, either uninjected (C), *tp53* MO (D), or *tp53* MO and *gata1a* MO (E). Injection of *gata1a* MO prevents the formation of erythroid cells (E). Lateral views, anterior to left. F: Quantification of *myl7* expression domain as a proxy for heart size in sibling and *lamb1a*^{Δ25} mutants, either uninjected (sibling: n=33; *lamb1a*^{Δ25} mutants: n=19), injected with *tp53* MO (sibling: n=29; *lamb1a*^{Δ25} mutant: n=20) or co-injected with *tp53* MO and *gata1a* MO (sibling: n=41; *lamb1a*^{Δ25} mutant: n=19) reveals that loss of erythroid cells through injection of *gata1a* MO does not rescue heart size in *lamb1a*^{Δ25} mutant embryos. All statistical analyses performed using Mann-Whitney test, **** = p < 0.0001, ns = not significant. Scale bars: 50μm.

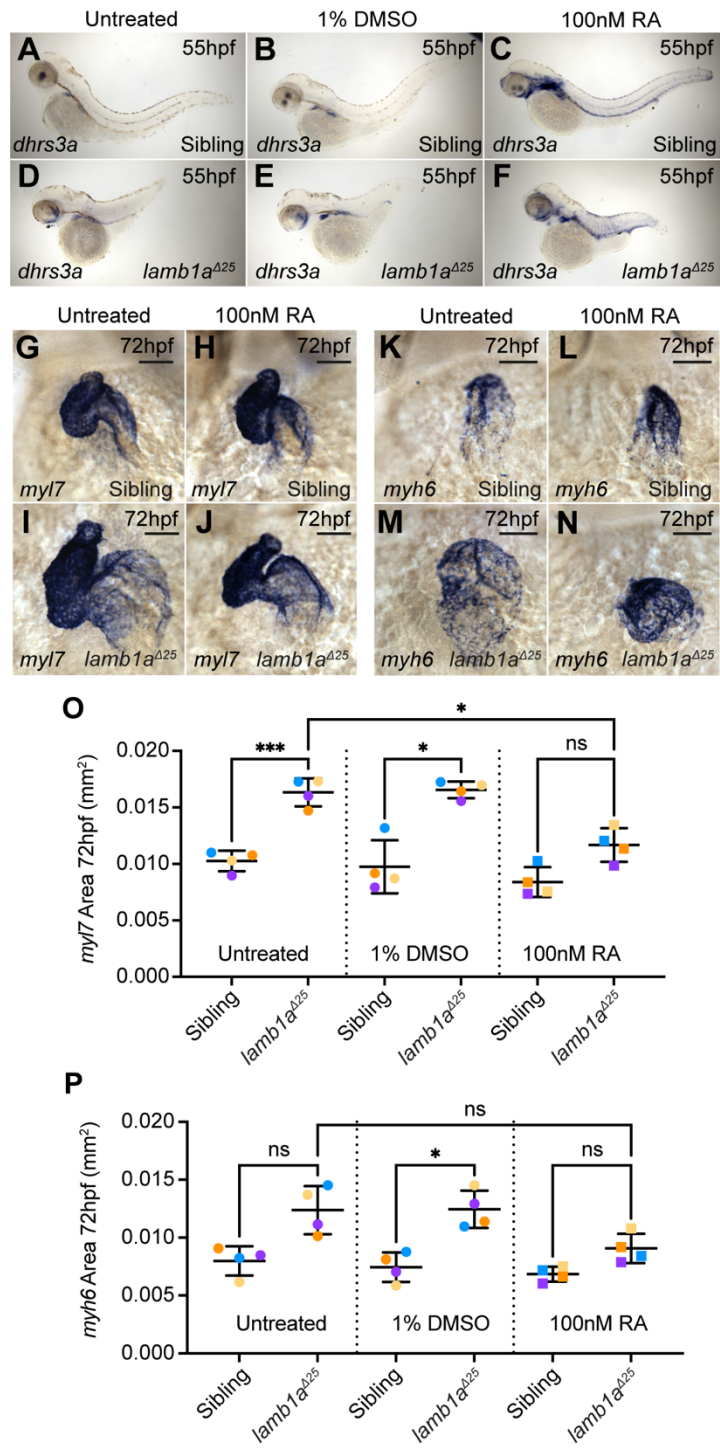


Fig. S9. Retinoic Acid treatment during SHF addition partially rescues cardiomegaly in *lambla* mutant embryos

A-F: mRNA *in situ* hybridization analysis of *dhrs3a* expression at 55hpf in sibling and *lambla*^{A25} mutants either untreated, incubated with DMSO, or incubated with 100nM RA from 24hpf to 55hpf. RA treatment results in an upregulation of the RA-responsive gene *dhrs3a* (C, F) compared to untreated controls (A,B,D,E). Lateral views, anterior to left). G-J: mRNA *in situ* hybridization expression analysis of *myl7* expression at 72hpf in sibling and *lambla*^{A25} mutant embryos, either untreated (G,I) or incubated in 100nM RA between 24hpf and 55hpf (H,J). K,N: mRNA *in situ* hybridization expression analysis of *myh6* at 72hpf in the atrium of sibling and *lambla*^{A25} mutant embryos, either untreated (K,M) or incubated in 100nM RA between 24hpf and 55hpf (L,N). Ventral views, anterior to top. O-P: Quantification of *myl7* expression domain (O) and *myh6* expression domain (P) in control and RA-treated embryos. RA treatment significantly reduces heart size in *lambla* mutants compared to controls (O). Median +/- interquartile range. All statistical analyses performed using Kruskal Wallis test, *** = $p < 0.001$, * = $p < 0.05$, ns = not significant. Scale bars: 50 μ m.

Table S1. primers and gene sequences used to generate novel in situ mRNA probes

Probe	Primer Sequence	Accession Number; ZFIN ID
<i>lama4</i>	F: 5'-CGATCAACTGCAGAGACACG-3'	ENSDARG00000020785; ZDB-GENE-040724-213
	R: 5'-GATGAACTTCTGCTCGGCTG-3'	
<i>lama5</i>	F: 5'-CCCTCGCACCAATACATGTG-3'	ENSDARG00000058543; ZDB-GENE-030131-9823
	R: 5'-CATTGGGTCTGCATCGACAG-3'	
<i>lamb1a</i>	F: 5'-TCCAATTACCCACCTCATC-3'	ENSDARG00000101209; ZDB-GENE-021226-1
	R: 5'-GGTCACAGTTCCTTCCGGTA-3'	
<i>lamb2</i>	F: 5'-CAAGACAACCGAAGCCAACA-3'	ENSDARG00000002084; ZDB-GENE-081030-4
	R: 5'-GGCTTACAGTCAGGGAAGGT-3'	
<i>lamc1</i>	F: 5'-GTGCTCTTGTAATCCAGCCG-3'	ENSDARG00000036279; ZDB-GENE-021226-3
	R: 5'-GCTCACATCGCTTACCTGTG-3'	
<i>islla</i>	F: 5'-GGACCTAACACCGCCTTACT-3'	ENSDARG00000004023; ZDB-GENE-980526-112
	R: 5'-TAGGACTCGCTACCATGCTG-3'	
<i>dhrs3a</i>	F: 5'-AAAGGTGATTTTGTGGGGCC-3'	ENSDARG00000044982; ZDB-GENE-040801-217
	R: 5'-ACAAGCCATCTCGATTCGC-3'	